國立交通大學

應用化學系分子科學碩士班
碩士論文

研究水溶解於 1,4-二氧陸圜的電場變調紅外線吸收光譜學

Infrared electroabsorbtion spectroscopic study of water in 1,4-dioxane

研究生：史習岡

指導教授：重藤真介　博士

中　華　民　國　一百　年　七　月

研究水溶解於 1,4-二氧陸圜的電場變調紅外線吸收光譜學

學生: 史習岡　　指導教授:重藤真介 博士

國立交通大學應用化學系分子科學碩士班

中文摘要

無論是靜態或動態的水都是一種複雜的液體，在本研究中我們用全新的觀點來討論靜態水分子對外加電場的反應。我們用電場變調紅外線吸收光譜來研究水溶解於 1,4-二氧陸圜的 O–H 伸縮振動範圍，我們的技術可以以高靈敏度偵測到外加電場對紅外線吸收光譜的變化，提供分子定量特性的分析，如永久偶極矩和可極化率等，而這些物性可以直接反應出分子的溶解結構和環境。

首先我們用多變量曲線分辨率方法分析水溶解於 1,4-二氧陸圜的濃度變化傅立葉轉換紅外線吸收光譜(濃度為 0-2M)，所觀察到的濃度依賴性光譜可經由假設兩個獨立的成分組合得到，我們命為單一水分子被 1,4-二氧陸圜包圍和自組的小群集水分子。接著我們偵測水溶解於 1,4-二氧陸圜的電場的紅外線吸收光譜(ΔA)，可成功測到ΔA 的訊號大小約為 10^{-6}。我們也測得一系列改變角度χ的ΔA 光譜，並用奇異值分析方法來分析，可成功分離出χ相關和χ不相關成分光譜，擬合光譜後的結果和目前為止對於其他液體分子的研究相比，本樣品對於電場回應的主要是由電子極化的貢獻(即偶極矩的變化和/或極化度的振動激發)，而非方向的取向異性貢獻。

Infrared electroabsorbtion spectroscopic study of water in 1,4-dioxane

Student: Shih, His-Kang Advisor: Dr. Shinsuke Shigeto

M. S. Program, Institute of Molecular Science, Department of Applied Chemistry, National Chiao Tung University

Abstract (in English)

Water is an exceedingly complicated liquid in both static and dynamic aspects. In the present study, we aimed to shed new light on the static molecular properties of water through investigating its response to an external electric field modulation. We studied the O–H stretch region of water dissolved in 1,4-dioxane using infrared (IR) electroabsorption spectroscopy. This technique is capable of detecting with high sensitivity the changes in IR absorption spectrum induced by an externally applied electric field. It provides quantitative information on molecular properties such as the permanent dipole moment and the polarizability, which sharply reflect the structure and local environments of the molecule.

First, using a multivariate curve resolution approach, we analyzed a series of FT-IR spectra of water dissolved in 1,4-dioxane at different concentrations of water ranging from 0 to 2 M. The results show that the observed concentration-dependent spectra can be reproduced well by assuming two independent components. We assigned these components as isolated water species surrounded by 1,4-dioxane and those in small water ensemble (cluster). Next, we measured IR electroabsorption (ΔA) spectra of the O–H stretch band of water dissolved in 1,4-dioxane. ΔA signal of the order of 10^{-6} was successfully detected. We recorded the ΔA spectrum by changing the angle, χ, between the direction of the applied field and the polarization vector of the IR light. The χ-dependence of the ΔA spectra was analyzed with a singular value decomposition approach, yielding the χ-dependent and χ-independent component spectra. Fitting analysis of both spectra suggests that, in contrast to other molecular liquids studied so far, water dissolved in 1,4-dioxane seems to respond to the electric field *via* the electronic polarization (*i.e.*, changes in dipole moment and/or polarizability upon vibrational excitation) rather than orientational anisotropy.

Acknowledgment

感謝這兩年來在交通大學的學業生活一切順利，感謝重藤真介老師的照顧和指導，提供實驗室良好的研究環境和儀器；感謝濱口宏夫老師也時常給予關鍵性的指導；感謝實驗室學長姐的照顧，現在回國工作的小宗時常幫忙實驗儀器維持，也常常教導儀器理論和數據分析，傳耿也常和我討論實驗內容和數據分析，威威教導我實驗操作；感謝同屆的同學偲偲、小阿芳、辰文和許智航的陪伴以及相互鼓勵；感謝學弟妹阿遠、apple、張君輔、何恭慧和李承翰讓實驗室充滿歡笑；感謝朋友給予我的鼓勵。最後，感謝我的爸媽和家人給予我很大的支持。

Tables of Contents

Page

List of Figures and Tables

Page

Chapter I

Introduction

Small molecules such as NH_3 and CH_4 exist as gas at ambient temperature and pressure. However, water is in its liquid phase under the ambient conditions. It is well-known that the boiling point of water is 100 ℃, which is unusually high compared to other molecules belonging to the same group in the periodic table (*e.g.*, H_2S, −61 °C; H_2Se, −41 °C). This and other physicochemical properties of water are mainly attributed to the presence of hydrogen bonds between water molecules. A water molecule is capable of forming four hydrogen bonds with neighboring water molecules (see Fig. I-1). Due to the three-dimensional network of hydrogen bonds, water is an exceedingly complicated liquid, and its anomalous properties are not yet fully understood.

Over many decades, tremendous efforts have been dedicated to understanding the molecular structure and dynamics of water [1-6]. Speaking of vibrational spectroscopy, one of the most remarkable characteristics of liquid water will definitely be the very broad O–H stretch band. Gaseous water exhibits two sharp bands at around 3755 and 3655 cm^{-1}, which are unambiguously assigned to the O–H antisymmetric and symmetric stretches, respectively. In contrast, liquid water shows an inhomogeneously broadened band with an approximate band width of 500 cm^{-1}. The broad O–H stretch band of water has been believed to consist of several vibrational subbands that reflect distinct hydrogen-bonding environments. The weaker the hydrogen bonding is, the bluer side the subband would appear at. Detailed information on the water species responsible for these subbands is a key to unravel the mystery of water. Given that different O–H subbands of water are associated with distinct hydrogen-bonding strengths, they are anticipated to respond to an externally applied electric field in a discrete manner *via* the orientational and electronic polarizations. The primary objective of the present work is to investigate the electric-field effects on the O–H stretch of water using infrared (IR) electroabsorption spectroscopy and to shed more light on the structure and electric properties of water.

Electrostatic interactions of molecules play a central role in chemistry. In liquid or solution, molecules are continuously exposed to electrostatic interactions with their surrounding, which may influence the direction and rate of chemical reactions. Fundamental molecular properties such as the permanent dipole moment, polarizability, and chemical bonding are also affected profoundly by electrostatic interactions. Therefore, electroabsoption spectroscopy (also known as Stark spectroscopy), which directly probes electrostatic interactions of molecules as responses to an external electric field, is a powerful technique for obtaining quantitative information on the molecular properties.

Electroabsorption spectroscopy provides unique information on molecular properties in diverse systems ranging from isolated gas-phase molecules to complex biological systems. The Stark effect [7-8] has been extensively studied in the visible region [9-11]. A series of pioneering work was done by Liptay and co-workers [12]. They demonstrated experimental determination of electric properties for many aromatic molecules in solution [12]. In addition, they developed a theoretical basis of Stark spectroscopy [13], which is now widely used in this field. Using frozen glasses at liquid N_2 temperature, Boxer and co-workers applied Stark spectroscopy to molecular systems such as donor–acceptor polyenes, transition metal complexes (metal-to-ligand and metal-to-metal mixed valence transitions), and nonphotosynthetic biological systems [10, 14]. They discussed quantitatively the amount of charge transfer based on two characteristic parameters obtained directly from experiment: the change in dipole moment, $\Delta\mu$, and the change in polarizability, $\Delta\alpha$, between the ground and excited *electronic* states. Experimental values of $\Delta\mu$ and $\Delta\alpha$ determined by Stark spectroscopy can also serve as a test for quantum chemical calculations [15]. Ohta and co-workers [9, 16-18] examined the electric-field effects on absorption and fluorescence spectra of polymer films with specific dopant molecules. For instance, they obtained $\Delta\mu$ and $\Delta\alpha$ of two different dopants (2-hydroxyquinoline and 6-hydroxyquinoline) embedded in a polymer film through

temperature dependence [18]. In another Stark study [17], they found that the photoirradiation of S3-PPV (sulfide-substituted PPV) in ambient air results in rapid degradation of the polymer film. These experimental results are useful when developing and designing novel optical devices.

Since vibrational spectra are sensitive to molecular structures, one can expect that electroabsorption in the mid-IR region is an excellent tool for studying the Stark effect in relation to structural properties of molecules. To our knowledge, the first *vibrational* Stark (IR electroabsorption) measurement is attributed to Handler and Aspnes [19]. As early as in 1967, they applied IR electroabsoption spectroscopy to study the Stark effect on the O–H stretch mode of 2,6-diisopropyl phenol in CCl_4 and obtained the parameters associated with the dipole moment and the polarizability of the phenol.

In 1995, Chattopadhyay and Boxer [20] reported the use of vibrational Stark spectroscopy to study the electric-field effect on the C≡N stretch mode of anisonitrile in toluene at 77 K. They evaluated $\Delta\mu$ and $\Delta\alpha$ between the vibrational states involved. The Boxer group extended their research to a series of compounds that contain the CN group [21]. In 2002 [22], they applied the technique to free CO and CO bound to myoglobin (Mb). It is shown that the change in dipole moment for the CO bound to Mb is larger than that for the free CO because of d–π* back-bonding. Extensive studies from the Boxer group have recently been reviewed [11].

These studies have all been performed with frozen glass at 77 K, where orientational motion of molecules is literally frozen or suppressed to a great extent. Under these experimental conditions, electroabsorption spectra can be more easily interpreted, because the electronic response *via* $\Delta\mu$ and $\Delta\alpha$ are only dominant contributions. However, those spectra are lacking in the information on the orientational response to an applied electric field, which is very useful for understanding molecular structures and association phenomena in

liquid/solution.

Hiramatsu and Hamaguchi developed an electroabsorption spectrometer in the IR region for room-temperature measurements [23]. Using a dispersive IR spectrometer equipped with an AC-coupled amplifier, instead of using the FT-IR method, they were able to detect IR absorbance changes as small as 10^{-7}. Hamaguchi and co-workers used their unique technique to investigate the *trans*/*gauche* conformational equilibrium of liquid 1,2-dichloroethane [24], followed by the studies of self-association of *N*-methylacetamide in 1,4-dioxane [25], association forms of a liquid crystal (5CB) at different temperatures [26], and solvated forms of *p*-nitroaniline (PNA) in mixed solvents of acetonitrile and CCl_4 [27]. In 2007, the whole system of the IR electroabsorption spectrometer was transferred to NCTU and reconstructed by our laboratory. Using the setup at NCTU, we have studied the *trans*/*gauche* conformational equilibrium and associated thermodynamic parameters of liquid 1,2-dibromoethane [28] and solvated structures of *N*,*N*-dimethyl-*p*-nitroaniline in mixed solvents of acetonitrile and tetrachloroethylene [29]. In the present work, the author extends the IR electroabsorption study to water dissolved in 1,4-dioxane, an aprotic solvent. As a first step of IR electroabsorption spectroscopy of pure water, which is technically challenging, the author dilutes water with 1,4-dioxane and investigates the electric-field effects on the O–H stretch vibration of dissolved water. Decreasing the absorption intensity of the O–H stretch makes it feasible to accurately detect absorbance changes of the O–H stretch band.

The rest of this thesis is organized as follows. In Chapter II, the theoretical background of IR electroabsorption spectroscopy is outlined. Major molecular responses to an externally applied electric field that contribute to IR absorbance changes are considered, and their mathematical expressions are derived. Chapter III provides details of our IR electroabsorption spectrometer and a home-made sample cell. Furthermore, spectral analysis using singular value decomposition (SVD) is briefly described as well. In Chapter IV, experimental results of

IR electroabsorption spectroscopy of water in 1,4-dioxane are presented and discussed. First, before discussing IR electroabsorption (ΔA) spectra, the concentration dependence of FT-IR absorption spectra of the sample is studied. It is found that the FT-IR spectra of water in 1,4-dioxane are well-explained by assuming two types of water components. Next, the ΔA spectra of water in 1,4-dioxane are presented. An important issue of the phase in lock-in detection is discussed in depth. The author measured the phase dependence of ΔA spectra in order to confirm the optimum phase retardation for the sample cell and the 1,4-dioxane solution of water. The electric-field-strength dependence of the ΔA spectra is then examined. Finally, the - dependent ΔA spectra and SVD analysis of the data are discussed in terms of the orientational and electronic polarization contributions. Here χ is the angle between the polarization vector of the IR probe light and the direction of the applied electric field. The conclusion is given in Chapter V.

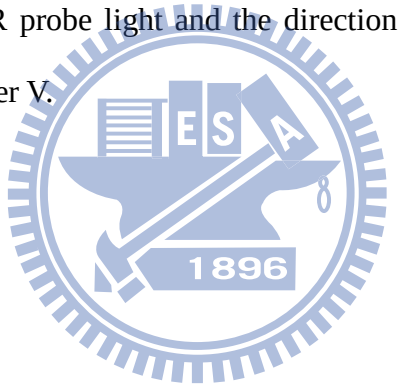

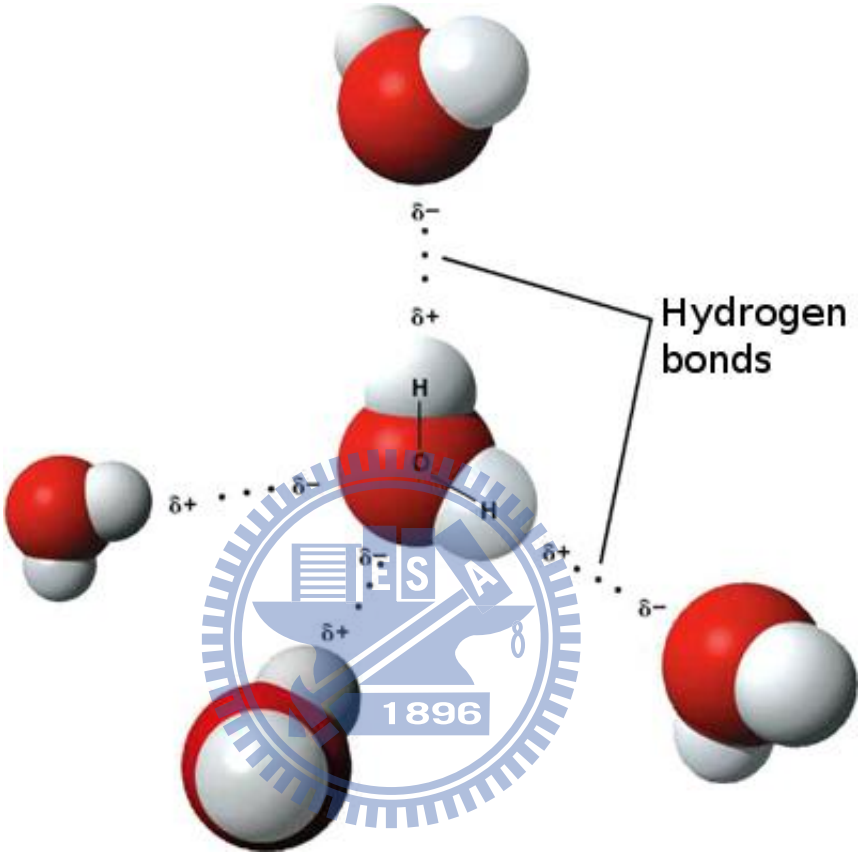

Figure I-1. Water molecule capable of forming four hydrogen bonds with neighboring water molecules.†

† http://en.wikipedia.org/wiki/File:3D_model_hydrogen_bonds_in_water.jpg

Chapter II

Theoretical background

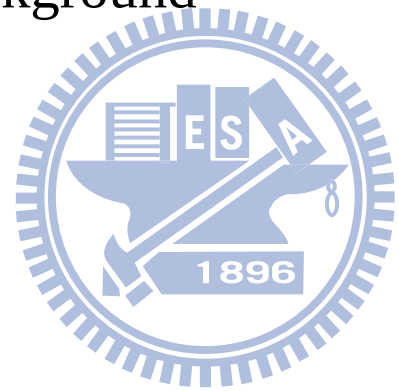

In this chapter, theoretical background of IR electroabsorption spectroscopy is described in detail. Some of the equations presented here will be used in Chapter IV to analyze experimental data. There are three distinct molecular responses to an externally applied electric field: orientational polarization, electronic polarization, and equilibrium shift. Mathematical expressions are derived for IR absorbance changes arising from these responses.

II-1. IR Absorbance difference (ΔA) spectra

When an electric field is externally applied to the sample, changes in absorption intensity are induced. The absorbance change (ΔA) is calculated from the intensity change ($\Delta I = I_{on} - I_{off}$) as follows:

$$\begin{aligned} \Delta A &= A_{on} - A_{off} \\ &= -\log\left(\frac{I_{on}}{I_0}\right) + \log\left(\frac{I_{off}}{I_0}\right) \\ &= -\log\left(1 + \frac{\Delta I}{I}\right) \end{aligned} \qquad \text{(II-1)}$$

Here I_0 represents the intensity spectrum of the IR probe light. I_{on} and I (= I_{off}) represent the intensity spectra of the transmitted IR light through the sample with and without the applied electric field, respectively.

II-2. Three distinct types of molecular responses

An absorbance change originates from different molecular responses to an applied electric field. Here, we consider three mechanisms of molecular responses to an externally applied electric field, namely, orientational polarization, electronic polarization, and equilibrium shift [24]. In what follows, we derive expressions for the ΔA spectrum arising from each molecular response and see how those molecular responses contribute to the overall ΔA spectrum.

II-2-a. Orientational polarization

Consider an ensemble of randomly-oriented polar molecules having a permanent dipole moment μ_p. Upon application of an external electric field, the dipole moments align along the direction of the electric field, giving rise to orientational anisotropy, although very small. This induced polarization can contribute to changes in absorption spectrum.

(1) Normally incident nonpolarized light

To derive an expression for the orientational polarization signal, let us begin with the Beer–Lambert law:

$$\begin{aligned} A &= \varepsilon cl \\ &= cl \cdot K\tilde{\nu}\int_0^{\pi} \sin\theta \mathrm{d}\theta \cdot f(\theta) \cdot \frac{1}{2\pi}\int_0^{2\pi} \mathrm{d}\varphi \cdot \frac{1}{2\pi}\int_0^{2\pi} \mathrm{d}\psi (\mathbf{e}\cdot\boldsymbol{\mu}_T)^2 \end{aligned} \qquad \text{(II-2)}$$

where ε is the molar extinction coefficient (L mol^{-1} cm^{-1}) , c is the concentration (mol L^{-1}), l is the path length (cm), K is a proportionality constant, $\tilde{\nu}$ is the wavenumber (cm^{-1}), and **e** is a unit vector designating the direction of the electric field of the incident light. In Figs. II-1 and II-2, we set the molecule-fixed coordinate system such that the z-axis coincides with the direction of the applied electric field and the propagation direction of the IR light. The orientations of the permanent dipole moment $\boldsymbol{\mu}_P$ and the transition moment $\boldsymbol{\mu}_T$ are specified by a set of angles (θ, φ, ψ). In Eq. II-2, there are two integrands to be evaluated explicitly; one is the spatial distribution function $f(\theta)$, and the other is the square of the inner product of the transition moment and the unit vector, $(\mathbf{e}\cdot\boldsymbol{\mu}_T)^2$.

The distribution function $f(\theta)$ is proportional to the probability of finding the dipole moment $\boldsymbol{\mu}_P$ in the direction θ with respect to the applied electric field **F**. Using the coordinate system shown in Figs. II-1 and II-2, we have

$$\boldsymbol{\mu}_{\mathrm{p}} = \mu_{\mathrm{p}} \begin{pmatrix} \sin\theta\cos\phi \\ \sin\theta\sin\phi \\ \cos\theta \end{pmatrix}, \ \mathbf{F} = F \begin{pmatrix} 0 \\ 0 \\ 1 \end{pmatrix}, \ \mathbf{e} = \begin{pmatrix} \cos\psi \\ \sin\psi \\ 0 \end{pmatrix} \tag{II-3}$$

The probability is proportional to $\exp\left(-\frac{E}{k_B T}\right)$, with E being the dipolar interaction energy

$$E = -\boldsymbol{\mu}_{\mathrm{p}} \cdot \mathbf{F} = -\mu_{\mathrm{p}} \begin{pmatrix} \sin\theta\cos\phi \\ \sin\theta\sin\phi \\ \cos\theta \end{pmatrix}^{\mathrm{T}} \cdot F \begin{pmatrix} 0 \\ 0 \\ 1 \end{pmatrix} = -\mu_{\mathrm{p}} F \cos\theta \tag{II-4}$$

Thus the distribution function $f(\theta)$ becomes

$$f(\theta) = C \exp\left(\frac{\mu_{\mathrm{p}} F \cos\theta}{k_B T}\right) = C \exp(\gamma \cos\theta) \tag{II-5}$$

with

$$\gamma = \frac{\mu_{\mathrm{p}} F}{k_B T} \tag{II-6}$$

Here C is a normalization factor, T is the temperature, and k_{B} is the Boltzmann constant, and F is the electric field strength. Note that the electric field F in Eq. II-6 is not the external field but *local* field which is actually exerted on individual molecules. The parameter γ reflects the magnitude of the electrostatic interaction. The factor C is determined by the normalization condition

$$\int_0^{2\pi} \int_0^{\pi} f(\theta) \sin\theta \, \mathrm{d}\theta \, \mathrm{d}\varphi = 1 \tag{II-7}$$

In the presence of the electric field ($F \neq 0$), $f(\theta)$ becomes from Eqs. II-5 and II-7

$$f^{\mathrm{on}}(\theta) = \frac{1}{2\pi} \frac{\gamma}{\exp(\gamma) - \exp(-\gamma)} \cdot \exp(\gamma \cos\theta) \tag{II-8}$$

In the absence of the electric field $(F = 0)$, we obtain $f(\theta)$ by taking the $\gamma \to 0$ limit of Eq.

$$f^{\mathrm{off}}(\theta) = \frac{1}{4\pi} \tag{II-9}$$

The scalar product of $\boldsymbol{\mu}_{\mathrm{T}}$ and **e** can be calculated as follows. The electric field vector **e**, of the incident light lies in the *xy*-plane, and a projection of $\boldsymbol{\mu}_{\mathrm{T}}$ onto the *xy*-plane is related to $(\boldsymbol{\mu}_{\mathrm{T}} \cdot \mathbf{e})^2$. $\boldsymbol{\mu}_{\mathrm{T}}$ is expressed as

$$\boldsymbol{\mu}_{\mathrm{T}} = |\mu_{\mathrm{T}}| \cdot \begin{pmatrix} -\cos\phi\cos\theta\cos\varphi\sin\alpha - \sin\phi\sin\varphi\sin\alpha + \cos\phi\sin\theta\cos\alpha \\ -\sin\phi\cos\theta\cos\varphi\sin\alpha + \cos\phi\sin\varphi\sin\alpha + \sin\phi\sin\theta\cos\alpha \\ \sin\theta\cos\varphi\sin\alpha + \cos\theta\cos\alpha \end{pmatrix} \tag{II-10}$$

If $\boldsymbol{\mu}_{\mathrm{P}}$ is parallel to $\boldsymbol{\mu}_{\mathrm{T}}$, *i.e.*, $\alpha = 0^{\circ}$ as shown in Fig. II-1, Eq. II-10 reduces to

$$\boldsymbol{\mu}_{\mathrm{T}} = \mu_{\mathrm{T}} \begin{pmatrix} \sin\theta\cos\phi \\ \sin\theta\sin\phi \\ \cos\theta \end{pmatrix} \tag{II-11}$$

Using Eqs. II-3 and II-11, $(\mathbf{e} \cdot \boldsymbol{\mu}_{\mathrm{T}})^2$ is obtained as

$$(\mathbf{e} \cdot \boldsymbol{\mu}_{\mathrm{T}})^2 = \frac{1}{2}\mu_{\mathrm{T}}^2 \sin^2\theta \tag{II-12}$$

Here we replace $\cos^2\psi$, $\sin^2\psi$, and $\cos\psi\sin\psi$ by their mean values evaluated for the range $0 \le \psi \le 2\pi$ (1/2, 1/2, and 1, respectively). In the absence of the external electric field, the absorbance A^{off} for an $\alpha = 0^{\circ}$ vibrational mode is calculated from Eqs. II-2, II-9, and II-12 as

$$\begin{aligned} A^{\mathrm{off}} &\propto \int_0^{2\pi}\int_0^{\pi} f^{\mathrm{off}}(\theta) \cdot \sin\theta \cdot |\mathbf{e} \cdot \boldsymbol{\mu}_{\mathrm{T}}|^2 \, \mathrm{d}\theta\mathrm{d}\phi \\ &= \frac{1}{4\pi} \cdot \frac{1}{2}\mu_{\mathrm{T}} \int_0^{2\pi} \sin^3\theta \mathrm{d}\theta\mathrm{d}\phi \\ &= \frac{1}{2}\mu_{\mathrm{T}}{}^2 \end{aligned} \tag{II-13}$$

Similarly, substitution of Eqs. II-8 and II-12 into Eq. II-2 results in the absorbance for the $\alpha = 0^{\circ}$ mode when the electric field is turned on

$$A^{\text{on}} \propto \int_0^{2\pi}\int_0^{\pi} f^{\text{on}}(\theta)\cdot\sin\theta\cdot\left|\mathbf{e}\cdot\boldsymbol{\mu}_{\text{T}}\right|^2 \mathrm{d}\theta\mathrm{d}\phi$$
$$= \frac{1}{2}\mu_{\text{T}}{}^2\cdot\frac{\gamma}{\mathrm{e}^{\gamma}-\mathrm{e}^{-\gamma}}\cdot\left[\frac{2}{\gamma^2}\left(\mathrm{e}^{\gamma}-\mathrm{e}^{-\gamma}\right)-\frac{2}{\gamma^3}\left(\mathrm{e}^{\gamma}-\mathrm{e}^{-\gamma}\right)\right] \qquad \text{(II-14)}$$

By expanding exponential functions in a Taylor series and retaining terms up to second-order in γ, we have

$$A^{\text{on}} \propto \frac{2}{\gamma^2+6}\cdot\mu_{\text{T}}{}^2 \qquad \text{(II-15)}$$

To confirm that this approximation is valid, suppose that a voltage of 50 V is applied across liquid acetone 5 μm thick. The electric field strength is $F = 1\times10^7\,\text{Vm}^{-1}$. For simplicity, we do not consider the local field correction. Using the dipole moment of acetone, μ_{P} = 2.7 D (1 D = 3.33564 × 10^{-30} C m), we obtain $\gamma = 0.02$, for which $\gamma << 1$ holds.

The absorbance change caused by the applied electric field is the difference between A^{on} (Eq. II-15) and A^{off} (Eq. II-13). The absorbance change ratio is thus

$$\frac{\Delta A}{A^{\text{off}}} = \frac{A^{\text{on}}-A^{\text{off}}}{A^{\text{off}}} = -\frac{\gamma^2}{\gamma^2+6} \qquad \text{(II-16)}$$

Next, we consider the $\alpha = 90°$ case, where $\boldsymbol{\mu}_{\text{T}}$ is perpendicular to $\boldsymbol{\mu}_{\text{P}}$ (Fig. II-2). Equation II-10 reduces to

$$\boldsymbol{\mu}_{\text{T}} = \mu_{\text{T}}\cdot\begin{pmatrix}-\cos\phi\cos\theta\cos\varphi-\sin\phi\sin\varphi\\-\sin\phi\cos\theta\cos\varphi+\cos\phi\sin\varphi\\\sin\theta\cos\varphi\end{pmatrix} \qquad \text{(II-17)}$$

and $(\mathbf{e}\cdot\boldsymbol{\mu}_{\text{T}})^2$ yields

$$(\mathbf{e}\cdot\boldsymbol{\mu}_{\text{T}})^2 = \frac{1}{4}\mu_{\text{T}}^2\left(\cos^2\theta+1\right) \qquad \text{(II-18)}$$

Making use of Eqs. II-2, II-8, II-9, and II-18, we end up with the absorbance change ratio of the form

$$\frac{\Delta A}{A^{\text{off}}} = \frac{\gamma^2}{2(\gamma^2+6)} \qquad \text{(II-19)}$$

Generalization of Eqs. II-16 and II-19 to an arbitrary angle α is straightforward. The

absorbance change for angle α can be decomposed into its parallel ($\alpha = 0^o$) and perpendicular ($\alpha = 90^o$) components as follows:

$$\Delta A_\alpha = \left(\frac{\Delta A}{A}\right)_{\alpha=0^o} \left|\mu_T \cos\alpha\right|^2 + \left(\frac{\Delta A}{A}\right)_{\alpha=90^o} \left|\mu_T \sin\alpha\right|^2 \qquad \text{(II-20)}$$

Substitution of Eqs. II-16 and II-19 into Eq. II-20 yields the following expression for the orientational polarization signal probed with the normal incidence

$$\Delta A_\alpha = \frac{\gamma^2}{2(\gamma^2+6)}\left(1-3\cos^2\alpha\right)\cdot A \qquad \text{(II-21)}$$

Again $\gamma^2 << 6$ in the present study, so the first term in the denominator of the right-hand side of Eq. II-21 is safely neglected. Therefore, we are left with

$$\frac{\Delta A_\alpha}{A} = \frac{\gamma^2}{12}\left(1-3\cos^2\alpha\right) \qquad \text{(II-22)}$$

(2) p-Polarized light with tilted incidence

So far we have considered the case where the electric field vector of the incident, nonpolarized light on the *xy*-plane is parallel to the sample cell. In other words, χ is equal to 90°, where χ is the angle between the applied electric field **F** and the electric field vector **e** of the incoming IR light (see Fig. II-3) When p-polarized light whose electric field vector **e** has only *x*-component is incident upon the sample with angle χ, the absorbance change ratio is shown to be given by [19]

$$\frac{\Delta A_{\alpha,\chi}}{A} = \frac{1}{12}\left(\frac{\mu_p F}{k_B T}\right)^2 \left(1-3\cos^2\alpha\right)\left(1-3\cos^2\chi\right) \qquad \text{(II-23)}$$

It follows from Eq. II-23 that the orientational polarization signal disappears at $\chi = \cos^{-1}\left(\sqrt{1/3}\right) = 54.7^o$. Furthermore the orientational polarization ΔA spectrum is proportional to the absorption spectrum *A*, so that it appears as its zeroth derivative (intensity change). An important implication of Eq. II-23 is that the dipole moment μ_P can be

experimentally determined from the zeroth derivative component of the ΔA spectrum [27, 29].

II-2-b. Electronic polarization

An absorbance change also arises from electronic polarization, which is associated with the changes in molecule's electronic properties such as the dipole moment and the polarizability. A general theory of the electronic polarization signal was established by Liptay and co-workers [12-13]. In general, the $\Delta A(\tilde{\nu})$ spectrum can be formulated as [30, 31]

$$\Delta A(\tilde{\nu}) = F^2\left[A_\chi A(\tilde{\nu}) + \frac{B_\chi}{15hc}\tilde{\nu}\frac{\mathrm{d}}{\mathrm{d}\tilde{\nu}}\frac{A(\tilde{\nu})}{\tilde{\nu}} + \frac{C_\chi}{30h^2c^2}\tilde{\nu}\frac{\mathrm{d}^2}{\mathrm{d}\tilde{\nu}^2}\frac{A(\tilde{\nu})}{\tilde{\nu}}\right] \qquad \text{(II-24)}$$

where h is Planck's constant and c is the speed of light. There are also third derivative and higher order terms in Eq. II-24, but they are all proportional to the fourth or higher powers of the electric field, which we do not detect. $\Delta A(\tilde{\nu})$ comprises the zeroth, first, and second derivatives of the absorption band $A(\tilde{\nu})$. For a randomly oriented, mobile molecule, the coefficients A_χ, B_χ, and C_χ are given by [30-32]

$$\begin{aligned} A_\chi = {} & \frac{1}{30|\mathbf{m}|^2}\sum_{ij}\left[10A_{ij}^{\ 2} + \left(3A_{ii}A_{jj} + 3A_{ij}A_{ji} - 2A_{ij}^{\ 2}\right)\left(3\cos^2\chi - 1\right)\right] \\ & + \frac{1}{15|\mathbf{m}|^2 k_\mathrm{B}T}\sum_{ij}\left[10m_iA_{ij}\mu_{gj} + \left(3m_iA_{ji}\mu_{gj} + 3m_iA_{jj}\mu_{gi} - 2m_iA_{ij}\mu_{gj}\right)\left(3\cos^2\chi - 1\right)\right] \\ & + \frac{1}{10k_\mathrm{B}T}\left(\alpha_{gm} - \overline{\alpha_g}\right)\left(3\cos^2\chi - 1\right) + \frac{\mu_g^{\ 2}}{30k_\mathrm{B}^2T^2}\left(3\cos^2\alpha - 1\right)\left(3\cos^2\chi - 1\right) \end{aligned} \qquad \text{(II-25)}$$

$$\begin{aligned} B_\chi = {} & \frac{1}{|\mathbf{m}|^2}\sum_{ij}\left[m_iA_{ij}\Delta\mu_j + \left(3m_iA_{ji}\Delta\mu_j + 3m_iA_{jj}\Delta\mu_i - 2m_iA_{ij}\Delta\mu_j\right)\left(3\cos^2\chi - 1\right)\right] \\ & + \frac{15}{2}\overline{\Delta\alpha} + \frac{3}{2}\left(\Delta\alpha_m - \overline{\Delta\alpha}\right)\left(3\cos^2\chi - 1\right) + \frac{5}{k_\mathrm{B}T}\left(\boldsymbol{\mu}_g\cdot\Delta\boldsymbol{\mu}\right) \\ & + \frac{1}{k_\mathrm{B}T}\left[3\left(\hat{\mathbf{m}}\cdot\boldsymbol{\mu}_g\right)\left(\hat{\mathbf{m}}\cdot\Delta\boldsymbol{\mu}\right) - \left(\boldsymbol{\mu}_g\cdot\Delta\boldsymbol{\mu}\right)\right]\left(3\cos^2\chi - 1\right) \end{aligned} \qquad \text{(II-26)}$$

$$C_\chi = 5|\Delta\boldsymbol{\mu}|^2 + \left[3\left(\hat{\mathbf{m}}\cdot\Delta\boldsymbol{\mu}\right) - |\Delta\boldsymbol{\mu}|^2\right]\left(3\cos^2\chi - 1\right) \qquad \text{(II-27)}$$

where the transition hyperpolarizability **B** is neglected. $\boldsymbol{\mu}_g$ is equal to $\boldsymbol{\mu}_p$. **A** denotes the transition polarizability. $\Delta\boldsymbol{\mu}$ and $\Delta\boldsymbol{\alpha}$ denote the changes in dipole moment and polarizability tensor between the vibrational ground state (g) and an excited state (e), respectively, *i.e.*, $\Delta\boldsymbol{\mu} = \boldsymbol{\mu}_e - \boldsymbol{\mu}_g$ and $\Delta\boldsymbol{\alpha} = \boldsymbol{\alpha}_e - \boldsymbol{\alpha}_g$. $\hat{\mathbf{m}}$ is a unit vector in the direction of the transition dipole moment **m** (for consistency with the literature, we prefer to use **m** for the transition moment instead of $\boldsymbol{\mu}_T$). α_{gm} and $\Delta\alpha_m$ are the components of the ground-state polarizability and the polarizability change along the direction of the transition moment, *i.e.*, $\alpha_{gm} = \hat{\mathbf{m}} \cdot \boldsymbol{\alpha}_g \cdot \hat{\mathbf{m}}$ and $\Delta\alpha_m = \hat{\mathbf{m}} \cdot \Delta\boldsymbol{\alpha} \cdot \hat{\mathbf{m}}$. A bar indicates the average value of the polarizability ($\overline{\alpha_g} = \frac{1}{3}\mathrm{Tr}\alpha_g$, $\overline{\Delta\alpha} = \frac{1}{3}\mathrm{Tr}\Delta\alpha$).

The zeroth-derivative component represents the *intensity change* of the absorption spectrum. Note that the fourth term in Eq. II-25 is essentially identical to the orientational polarization contribution, which we already derived above. The first-derivative component depends on both $\Delta\boldsymbol{\mu}$ and $\Delta\boldsymbol{\alpha}$ and is responsible for the *peak shift*, as illustrated in Fig. II-4. The second-derivative component, which is characterized solely by $\Delta\boldsymbol{\mu}$, shows the *change in the band width* of the absorption spectrum (see Fig. II-5).

II-2-c. Equilibrium shift

A shift of chemical equilibrium caused by an external electric field can also contribute to the ΔA signal. If the electrostatic interaction differs among molecular species coexisting in equilibrium, the equilibrium would shift towards more stable species [24, 28]. Here let us take 1,2-dicholoroethane as an example for better understanding of such ΔA signal. In 1,2-dicholoroethane, the *trans* and *gauche* conformers coexist in equilibrium. The *trans* conformer is nonpolar, while the *gauche* is polar. When an electric field is applied to the liquid, the *gauche* conformer gets stabilized *via* the electrostatic (dipolar) interaction. On the

other hand, the nonpolar *trans* conformer is not affected by the electric field. As a result, the equilibrium shifts towards the *gauche* conformer. Thus IR absorption of the *gauche* conformer is expected to increase, while that of the *trans* conformer should decrease.

Since this equilibrium shift ΔA signal is a change in absorption intensity, it has the same shape as the absorption spectrum and hence contributes to the zeroth-derivative component as is the orientational polarization signal. However, the equilibrium shift signal is independent of the angle χ. It is thus possible to distinguish between the orientational polarization and equilibrium shift contributions to the ΔA spectrum through angle χ dependence of the ΔA spectrum.

II-3. Conclusion

In this chapter, the theoretical basis for IR electroabsorption spectroscopy has been introduced. IR electroabsorption signals appear as the changes in intensity, peak position, and band width of the absorption band. Equations II-24–27 are employed for data analysis in Chapter IV.

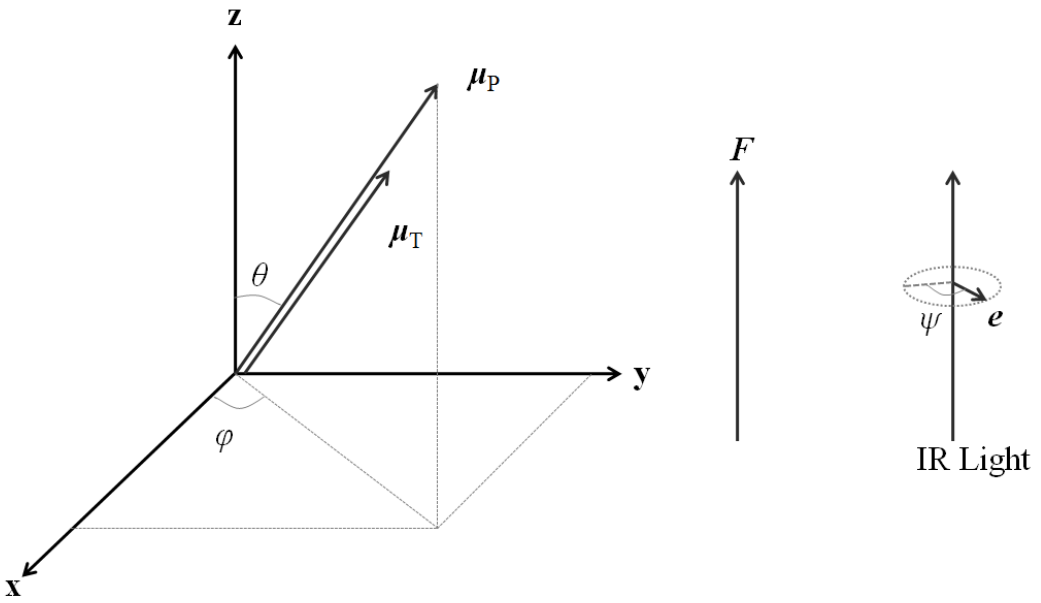

Figure II-1. Coordinate system used in derivation of the orientational polarization signal. α is the angle between $\boldsymbol{\mu}_P$ and $\boldsymbol{\mu}_T$. This figure corresponds to the $\alpha = 0°$ case, where $\boldsymbol{\mu}_P$ is parallel to $\boldsymbol{\mu}_T$.

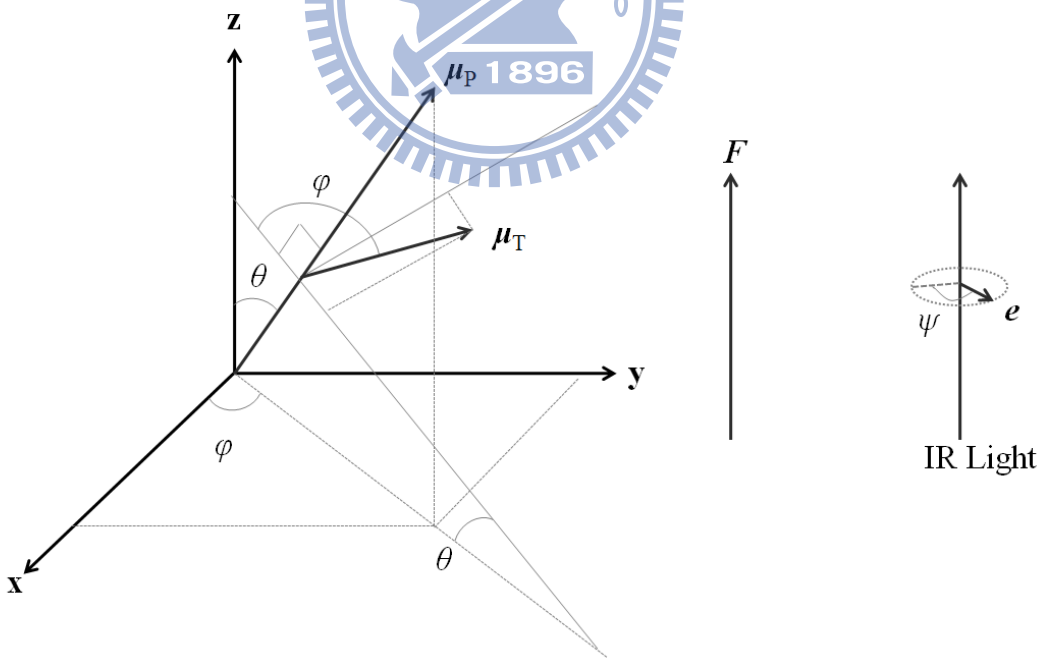

Figure II-2. Coordinate system used in derivation of the orientational polarization signal. This figure corresponds to the $\alpha = 90°$ case, where $\boldsymbol{\mu}_P$ is perpendicular to $\boldsymbol{\mu}_T$.

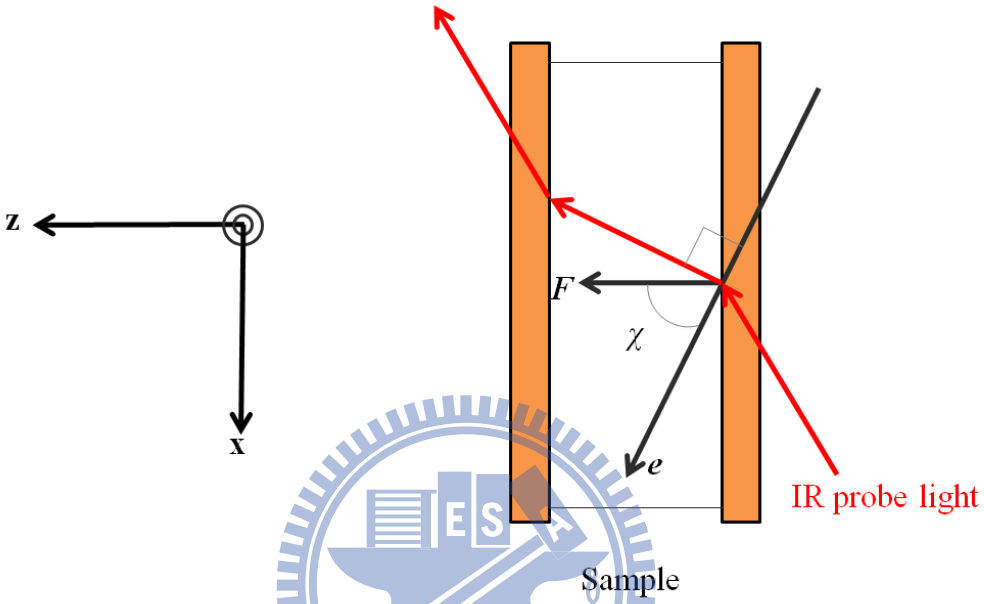

Figure II-3. Angle χ between the applied electric field **F** and the electric field vector **e** of the incoming IR probe light.

(a)

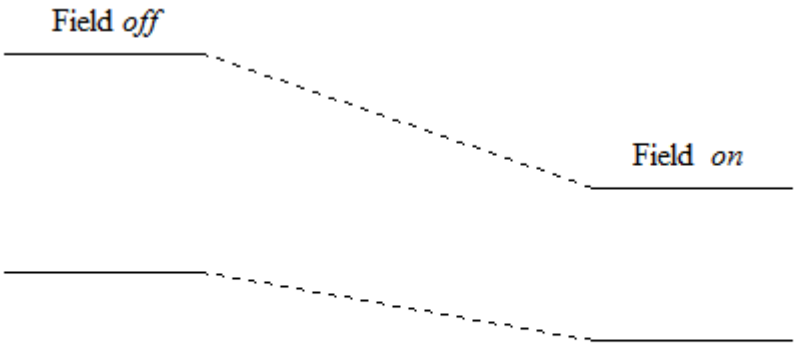

(b)

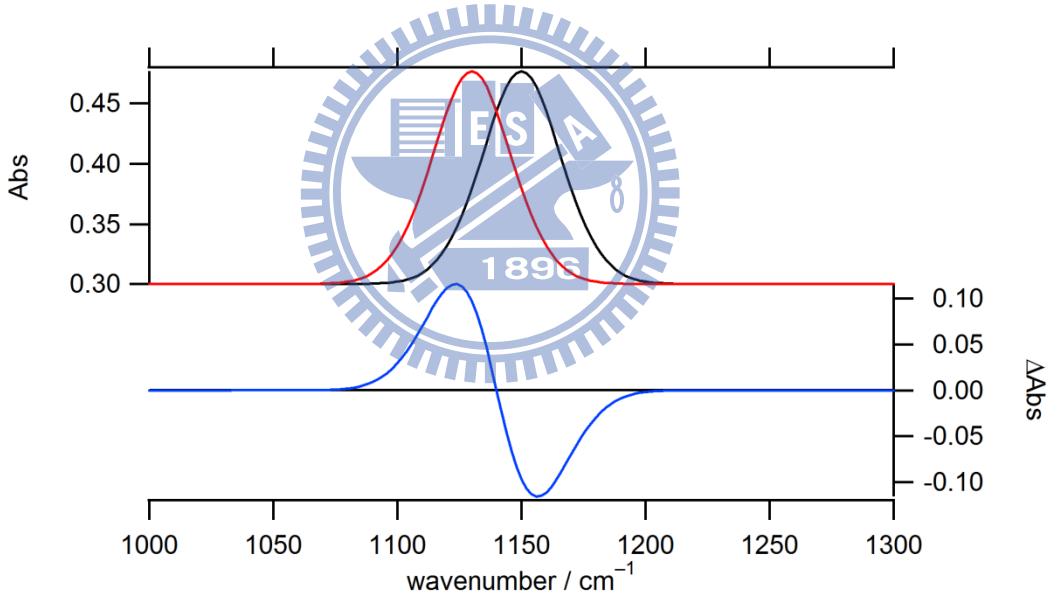

Figure II-4. (a) Electric field effect in the vibrational ground and excited states. (b) An absorption peak shifts to the lower frequency (black → red), and the resulting ΔA spectrum (blue line) exhibits a first derivative line shape. $\Delta\alpha > 0$ causes such a lower wavenumber shift.

(a)

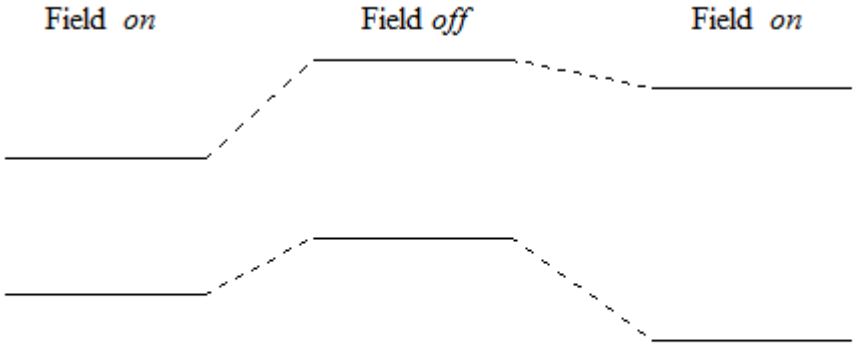

(b)

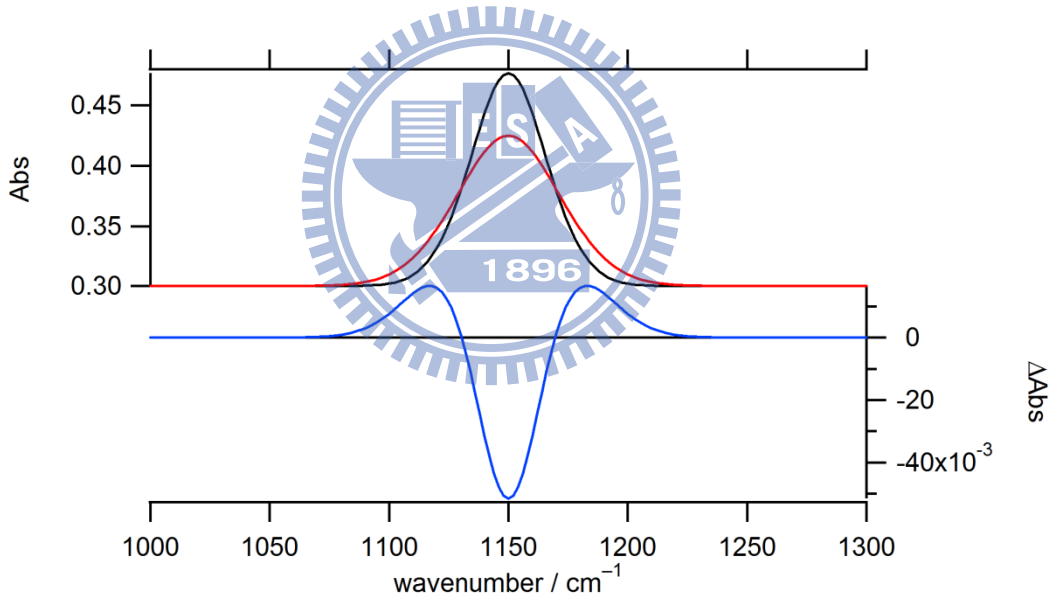

Figure II-5. (a) Electric field effect on the distribution of the $v = 1 \leftarrow 0$ transition frequency. (b) An absorption peak is broadened (black → red), and the resulting ΔA spectrum (blue line) shows a second derivative line shape. $\Delta\mu$ is responsible for such a broadening.

Chapter III

Experiment and Analysis

The apparatus for IR electroabsoption spectroscopy used in the present study was originally developed by Hiramatsu and Hamaguchi [23] and subsequently reconstructed at NCTU by us. The principle of IR electroabsorption spectroscopy and our experimental setup are described in this chapter, followed by the details of our home-built sample cell. It is highlighted that, owing to a combination of a dispersive spectrometer and an AC-coupled amplification technique, the detection limit of absorbance change is as low as $\Delta A \sim 10^{-7}$. Sample preparation for IR electroabsorption and FT-IR measurements are also described. An analytical method for ΔA spectra using singular value decomposition (SVD) is also presented in this chapter with some mathematical accounts.

III-1. Experimental setup—IR electroabsorption spectrometer

The experimental setup for IR electroabsorption spectroscopy is described in this section. A schematic of the experimental setup is shown in Fig. III-1. The system consists of a light source, a home-built sample cell, an optical chopper (Stanford Research System Inc. SR540), a dispersive IR monochromator, a photoconductive InSb detector (Kolmar Technologies, KISDP-1-J1/DC), an AC-coupled amplifier, and a lock-in amplifier (Stanford Research System Inc., SR844). The probe light source used to illuminate the sample was a ceramic mid-IR emitter (JASCO). As shown in Fig. III-1, the optical chopper and the sample cell were set at the co-focus of two ellipsoidal mirrors and at the other focus of the second ellipsoidal mirror, respectively. A chopper blade with 6 windows generated a modulation of 240 Hz to the probe light. A function generator (IWATSU, FG-330) produced a 25 kHz sinusoidal wave and, after amplified by a power amplifier, the AC voltage was applied across the sample about 6 μm thick. By combining the dispersive IR monochromator and the AC-coupled technique, the sensitivity to absorbance changes induced by electric field modulation can reach as high as 1×10^{-7}, which is better than that achieved by the latest FT-IR method. The spectral resolution was 8 cm^{-1} for all ΔA measurements.

In this paragraph, the AC-coupled technique is briefly outlined. It is a powerful technique to detect a small AC component lying on top of a large DC offset. In the present case, the intensity of the transmitted IR probe light corresponds to the DC offset and an intensity change due to electric field modulation is the AC component [Fig. III-2(a)]. The amplitude of the AC component is typically three or even higher orders of magnitude smaller than that of the DC offset. In order to detect such small AC amplitude, we used a low-noise preamplifier to remove the DC offset [Fig. III-2(b)] and amplified only the AC component. Then the output of the preamplifier was amplified once again [Fig. III-2(c)] by the main amplifier [Stanford Research System Inc. SR560, gain 1–5000 (variable)] and fed by the lock-in amplifier. In this way, only the intensity change due to electric field modulation can be detected with a wide dynamic range.

In electroabsorption measurements, three spectra are measured. (i) The intensity spectrum, I_0, of the IR probe light without the sample. (ii) The intensity spectrum, I, of the IR probe light with the sample. I_0 and I are obtained using a digital sampling oscilloscope (LeCroy, LC334-DSO) and the mechanical chopper operating at about 240 Hz. In these measurements, no electric field is applied across the sample. (iii) The AC-coupled detection technique combined with a lock-in amplifier is employed to detect the intensity difference spectrum, ΔI, recorded with an electric field turned on. The ΔA spectrum is computed using Eq. II-1. In the following chapters, we will present our data in the format of ΔA spectra.

IR absorption spectra were also recorded on a JASCO FT/IR-6100 spectrometer. using a sample cell composed of two CaF_2 windows and a lead spacer (thickness = 25 μm). 64 runs were averaged for each IR absorption spectrum, and a wavenumber resolution of 8 cm^{-1} was used.

III-2. Sample cell

The configuration of our home-built sample cell is schematically shown in Fig. III-3. The sample cell consists of a brass cell holder (A/A') , two Si windows (B/B'), and a polyethylene terephthalate (PET) thin film (C) as a spacer. The PET film (Diafoil®) was a gift from Mitsubishi Plastics. The Si windows used (Pier Optics) were p-type boron doped Si plates (resistivity = 0.8–2 Ω cm), so they also serve as electrodes. Because one side of the Si window was coated by a SiO_2 layer (thickness = 0.3 μm, resistivity $>10^{10}$ Ω cm), the electrodes were electrically insulated from the sample. The resulting transmission of the Si wafers is about 60% in the mid-IR region. The thickness of the PET film must be thin enough to avoid using high voltages, and a 6 μm film was our choice of the spacer. Between A' and B', we put chemically durable perfluoroelastmer O-rings (As568A-008) to prevent a liquid sample from leaking out of the flow system during measurement. Flowing the sample was required in order to avoid sample evaporation.

Accurate estimation of the cell gap and the applied voltage is essential for calculating the external electric-field strength. We can estimate the actual cell gap from an interference fringe pattern that appears in the absorption spectrum of a vacant cell. The peak positions of two adjacent peaks of an interference fringe pattern, ω_1 and ω_2 (cm^{-1}), are related to the cell gap a (μm) as

$$2n_{\omega_1}a = \frac{10^4}{\omega_1} \times \frac{2m-1}{2} \qquad \text{(III-1)}$$

$$2n_{\omega_2}a = \frac{10^4}{\omega_2} \times \frac{2m+1}{2} \qquad \text{(III-2)}$$

where $n_{\omega 1}$ and $n_{\omega 2}$ are refractive indices at ω_1 and ω_2, respectively, and m is an integer. Assuming that $n_{\omega_1} = n_{\omega_2}$, the cell gap a is obtained as

$$a = \frac{1}{2} \times \frac{10^4}{\omega_2 - \omega_1} \qquad \text{(III-3)}$$

In order to suppress unwanted work at the cell caused by nonzero resistance between A-A' ($V_{AA'}$) and B-B' ($V_{BB'}$), we should decrease the contact resistance between them as small as possible. We scratched the surface of the Si plate at two points with a distance of ~2 cm to physically remove the naturally coated SiO_2 layer. On those points was pasted indium-gallium alloy (Ga 40%), making electric contacts with the brass cell holder. The resistance between the two points was nominally smaller than ~20 Ω. It depends on the doping properties of the Si plates. A large resistance may give rise to a decrease in amplitude of the applied voltage and phase retardation with respect to the applied sinusoidal wave. The latter may result in nonzero out-of-phase ΔA signals. This phenomenon has been explained by regarding the sample cell as forming an RC circuit [23]. Figure III-4 shows an RC circuit equivalent to the sample cell. R_1 and R_2 are the resistances between A and B and between A' and B', respectively, and C_C is the capacitance between the electrodes. The exact voltage across the sample ($V_{BB'}$) is related to the applied voltage ($V_{AA'}$) as [18]

$$V_{BB'} = V_{AA'} \frac{1}{\sqrt{1+(\omega R C_C)^2}} \left[\frac{1}{\sqrt{1+(\omega R C_C)^2}} + \mathrm{i} \frac{\omega R C_C}{\sqrt{1+(\omega R C_C)^2}} \right] \qquad \text{(III-4)}$$

where $R = R_1 + R_2$, i is the imaginary unit, ω is the angular frequency of the electric field which we apply. The amplitude and the phase retardation are thus given by

$$\text{Amplitude} = \frac{V_{AA'}}{\sqrt{1+(\omega R C_C)^2}}, \qquad \text{(III-5)}$$

$$\text{Retardation} = \arctan(\omega R C_C) \qquad \text{(III-6)}$$

respectively. This problem becomes more serious as the ωRC_C term becomes larger. The

capacitance C_C varies depending on the concentration and the dielectric constant of the sample.

The magnitude of an externally applied electric field, F_{ext}, can be calculated from the applied voltage and the cell gap. However, F_{ext} is not the exact field strength that acts on the molecules in the sample. It is the local field F_{local} that is actually exerted on the molecules [23]. Therefore we need to consider the relation between the local and external electric fields. The local electric field F_{local} is related to the external field as

$$F_{local} = f' \cdot f'' \cdot F_{ext} \qquad \text{(III-7)}$$

Here the factor f' is given by

$$f' = \frac{1}{\sqrt{1+(\omega RC_C)^2}}\left[\frac{1}{\sqrt{1+(\omega RC_C)^2}} + i\frac{\omega RC_C}{\sqrt{1+(\omega RC_C)^2}}\right] \qquad \text{(III-8)}$$

which accounts for the effect of the RC circuit that the sample cell may form, and f'' is the local-field correction. It is often very difficult to evaluate the factors f' and f'' accurately. According to the Onsager theory, for instance, the local-field correction is given by

$$f'' = \frac{3\varepsilon_r}{2\varepsilon_r + 1} \qquad \text{(III-9)}$$

where ε_r is the dielectric constant of the medium. By definition, ε_r takes on values from unity to infinity, resulting in the value of f'' between 1.0 and 1.5. However, this theory is based on a simple model of intermolecular interactions and liquid structures, and there are many limitations to broad applications. Thus, values of molecular properties are often quoted in the units of f'' in previous studies [34-35].

III-3. Sample preparation

Molecular sieves (Type 3Å , 8–12 mesh, J. T. Baker) were put into 1,4-dioxane (>99%, J. T. Baker) in order to remove residual water, followed by filtration (pore size = 0.2 μm) in

order to remove dusts or particles in 1,4-dioxane. We dissolved deionized water in 1,4-dioxane at concentrations of 0.050, 0.10, 0.15, 0.20, 0.25, 0.30, 0.35, 0.40, 0.50, 0.75, 1.0, 1.25, 1.50, 1.75, and 2.0 M for FT-IR measurements. These molar concentrations correspond to water mole fractions of 0.042, 0.085, 0.013, 0.017, 0.021, 0.025, 0.029, 0.033, 0.041, 0.060, 0.079, 0.096, 0.11, 0.13, and 0.15. We used 1.0 M for IR electroabsorption measurements.

III-4. Analytical method—singular value decomposition

Singular value decomposition (SVD) is an important factorization method of a complex matrix. This technique can be employed in principal component analysis (PCA); thus it has found many applications in chemometrics and spectral analysis.

SVD is a rigorous mathematical method that decomposes an arbitrary (complex) matrix **X** ($m \times n$, $m > n$) into the product of three matrices **U**, **W**, and **V** as

$$\mathbf{X} = \mathbf{U}\mathbf{W}\mathbf{V}^{\mathrm{T}} \qquad \text{(III-10)}$$

where **U** is a column-orthogonal matrix ($m \times n$), **W** is a diagonal matrix ($n \times n$), and **V** is a real orthogonal matrix ($n \times n$). The diagonal elements of the matrix **W** are called singular values. Equation III-10 can be explicitly written in terms of matrix elements:

$$\begin{bmatrix} X_{11} & \cdots & X_{1n} \\ \vdots & \ddots & \vdots \\ X_{m1} & \cdots & X_{mn} \end{bmatrix} = \begin{bmatrix} U_{11} & \cdots & U_{1n} \\ \vdots & \ddots & \vdots \\ U_{m1} & \cdots & U_{mn} \end{bmatrix} \begin{bmatrix} W_1 & 0 & 0 \\ 0 & \ddots & 0 \\ 0 & 0 & W_n \end{bmatrix} \begin{bmatrix} V_{11} & \cdots & V_{1n} \\ \vdots & \ddots & \vdots \\ V_{n1} & \cdots & V_{nn} \end{bmatrix} \qquad \text{(III-11)}$$

The column vector $\left(U_{1k} \cdots U_{mk}\right)^{\mathrm{T}}$ is denoted $\mathbf{u}_k$ $\left(k = 1, \cdots, n\right)$, and the row vector $\left(V_{k1} \cdots V_{kn}\right)$ denoted $\mathbf{v}_k$ $\left(k = 1, \cdots, n\right)$. Equation III-11 is then simplified to

$$\mathbf{X} = \begin{bmatrix} \mathbf{u}_1 & \cdots & \mathbf{u}_n \end{bmatrix} \begin{bmatrix} W_1 & 0 & 0 \\ 0 & \ddots & 0 \\ 0 & 0 & W_n \end{bmatrix} \begin{bmatrix} \mathbf{v}_1 \\ \vdots \\ \mathbf{v}_n \end{bmatrix} \qquad \text{(III-12)}$$

Let the matrix **X** represent a set of time-resolved spectra with a row corresponding to the spectrum observed at a given time. In this case, $\mathbf{u}_k$ represents a time dependence, while $\mathbf{v}_k$ corresponds to the intrinsic spectrum for the *k*th component. Contributions of the *k*th component to the overall matrix **X** are determined by the singular value W_k: the larger W_k is, the more significantly the *k*th component contributes. The usefulness of SVD stems from the fact that components with small singular values can be neglected.

How does SVD analysis work? Consider the following two cases typically encountered in spectral analysis using SVD: (1) SVD yields only one or two major singular values [see Fig. III-5(a)]. (2) SVD yields several non-negligible singular values [Fig. III-5(b)].

In case 1 [Fig. III-5(a)], the presence of the two major singular values indicates that, in principle, two and only two molecular species are responsible for the original data set (matrix **X**). Such a case can be found, for example, when performing the SVD of a series of absorption spectra in which absorption band 1 increases and concomitantly another band 2 decreases as a function of concentration. We are able to disregard all the other singular values and to focus on the behavior of the two components 1 and 2. Mathematically, this simplification implies

$$\mathbf{X} \approx \begin{bmatrix} \mathbf{u}_1 & \mathbf{u}_2 \end{bmatrix} \begin{bmatrix} W_1 & 0 \\ 0 & W_2 \end{bmatrix} \begin{bmatrix} \mathbf{v}_1 \\ \mathbf{v}_2 \end{bmatrix} \qquad \text{(III-13)}$$

Now that we are left with much reduced number of components, we can proceed to assign physical meanings to components 1 and 2. It should be noted that SVD is a purely mathematical operation and hence there are no physical meanings attached to vectors **u** and **v** as they stand. Those vectors need to be reconstructed by taking linear combinations of **u** and **v**. At this stage, physics (or chemistry) behind the observed phenomenon comes into play. In order to obtain physically meaningful vectors **u**′ and **v**′, we need to assume model functions that **u** and **v** are expected to obey. By way of example, in the SVD analysis of χ-dependent IR

electroabsorption spectra [27], the model functions for the χ-dependent and χ-independent components have been assumed to be $1-3\cos^2\chi$ and constant with respect to χ, respectively. Mathematically, this reconstruction corresponds to inserting the product of a transformation matrix **K** and its inverse $\mathbf{K}^{-1}$ between matrices **U** and **W**, namely, inserting a unit matrix **E** = $\mathbf{K}\mathbf{K}^{-1}$. The matrix elements of **K** are determined by least-squares fitting to the model functions.

$$\mathbf{X} \approx \begin{bmatrix}\mathbf{u}_1 & \mathbf{u}_2\end{bmatrix}\mathbf{K}^{-1}\mathbf{K}\begin{bmatrix}W_1 & 0\\ 0 & W_2\end{bmatrix}\begin{bmatrix}\mathbf{v}_1\\ \mathbf{v}_2\end{bmatrix} = \begin{bmatrix}\mathbf{u}'_1 & \mathbf{u}'_2\end{bmatrix}\begin{bmatrix}\mathbf{v}'_1\\ \mathbf{v}'_2\end{bmatrix} \qquad \text{(III-14)}$$

where

$$\begin{bmatrix}\mathbf{u}'_1 & \mathbf{u}'_2\end{bmatrix} = \begin{bmatrix}\mathbf{u}_1 & \mathbf{u}_2\end{bmatrix}\mathbf{K}^{-1},$$
$$\begin{bmatrix}\mathbf{v}'_1\\ \mathbf{v}'_2\end{bmatrix} = \mathbf{K}\begin{bmatrix}W_1 & 0\\ 0 & W_2\end{bmatrix}\begin{bmatrix}\mathbf{v}_1\\ \mathbf{v}_2\end{bmatrix} \qquad \text{(III-15)}$$

In case 2, there are many (typically more than three) singular values with non-negligible amplitudes, as shown in Fig. III-5(b). Such a plot is characteristic of the data in which one component undergoes a continuous shift as a function of a variable such as concentration or time. If an absorption band continuously shifts from red to blue or *vice versa* with concentration, a plot of the singular values so obtained resembles Fig. III-5(b). In comparison with case 1, SVD analysis is silent in this case. However, it does provide important information on whether the observed data arise from a few components in equilibrium or a single, continuously changing component.

III-5. Electroabsorption (ΔA) and intensity difference (ΔI) spectra

In this section, we would like to demonstrate how the presence of an offset in the ΔI spectrum that is possibly caused by the electronics results in artifacts in the ΔA spectrum. As already described in Chapter II, the ΔA spectrum is calculated from the ΔI spectrum according to Eq. II-1. Equation II-1 shows that the ΔA signal depends not only on ΔI but also on I. This

fact may give rise to artificial ΔA peaks although there is no intensity change of an IR transition induced by an electric field. Suppose that there is a vibrational band at 1150 cm^{-1}. It appears as a dip in the intensity (I) spectrum [Fig. III-6(a)]. Here, we consider four different types of the ΔI spectrum [Fig. III-6(b)]: (i) Neither ΔI signal nor an offset, namely, $\Delta I = 0$ (red spectrum). (ii) There is an absorption intensity change of -4.4×10^{-7} at 1150 cm^{-1} without any offset (purple spectrum). This is the ideal case. (iii) The ΔI spectrum contains both constant offset of 5×10^{-7} and absorption intensity change of -4.4×10^{-7} at 1150 cm^{-1} (blue spectrum). (iv) The ΔI spectrum contains a constant offset of 8×10^{-7} but no absorption intensity change at 1150 cm^{-1} (green spectrum). Unfortunately, we sometimes encounter cases iii and iv, producing an unwanted distortion of the spectrum or emergence of an artifact.

In each case, the ΔA spectrum is simulated by using Eq. II-1. The resulting ΔA spectra for the four cases are displayed in Fig. III-6(c). Needless to say, in case i, there is no ΔA signal everywhere. In case ii, a positive peak is observed at 1150 cm^{-1}, which is what we want to obtain in actual experiments. In case iii, a positive peak is still seen on top of an offset of $\sim 2 \times 10^{-6}$. It should be noticed, however, that the peak height at 1150 cm^{-1} is somewhat diminished compared to that in case ii. Furthermore, the peak at 1150 cm^{-1} accompanies tiny dips at both edges. These features showing up in the ΔA spectrum should have no molecular origin because the corresponding ΔI spectrum shows no such features. What is worse, the ΔA spectrum of case iv displays a *negative* peak of similar amplitude at 1150 cm^{-1}. Clearly, this negative peak is an artifact; there is no absorption intensity change in the ΔI spectrum [see Fig. III-6(b), green line].

The simple simulation mentioned above gives an important caveat: if one does not monitor the ΔI spectrum and focus exclusively on the ΔA spectrum, one may be fooled by an artifact originating from an offset in the ΔI spectrum and hence reach a false conclusion regarding the electric-field effects on the molecule. Therefore, it is crucial to confirm that the

ΔI spectrum shows intensity changes at vibrational transition frequencies before interpreting the ΔA spectrum.

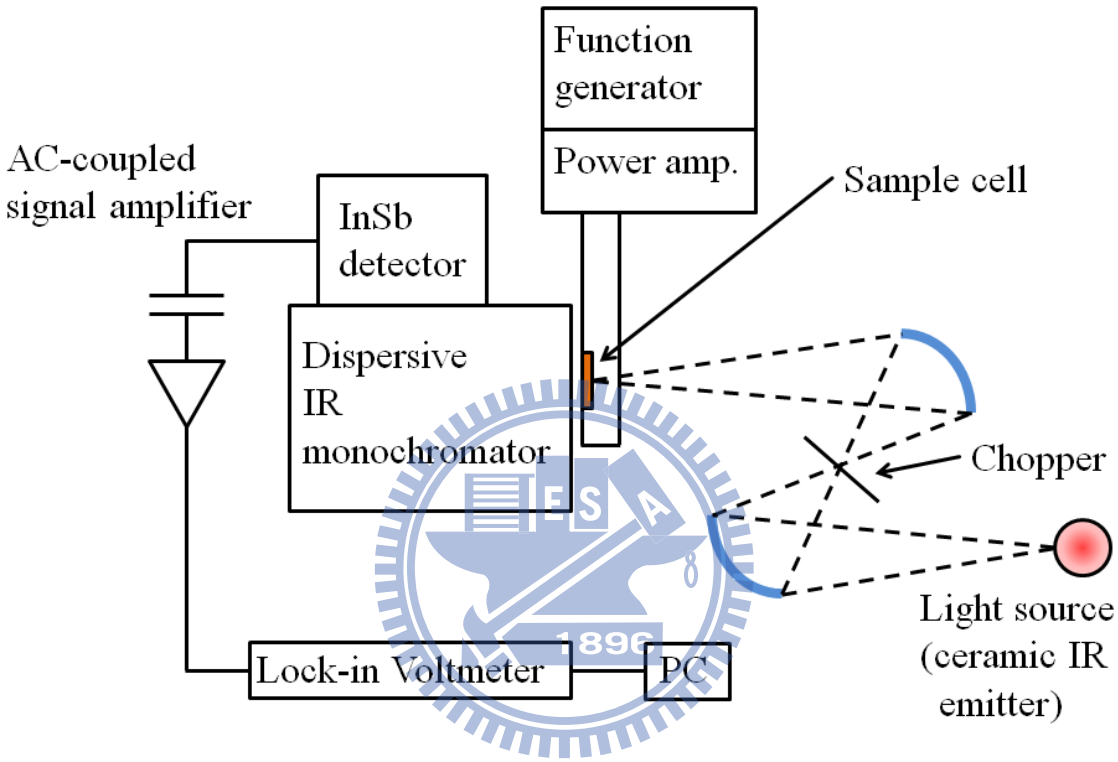

Figure III-1. Experimental setup of IR electroabsorption spectroscopy.

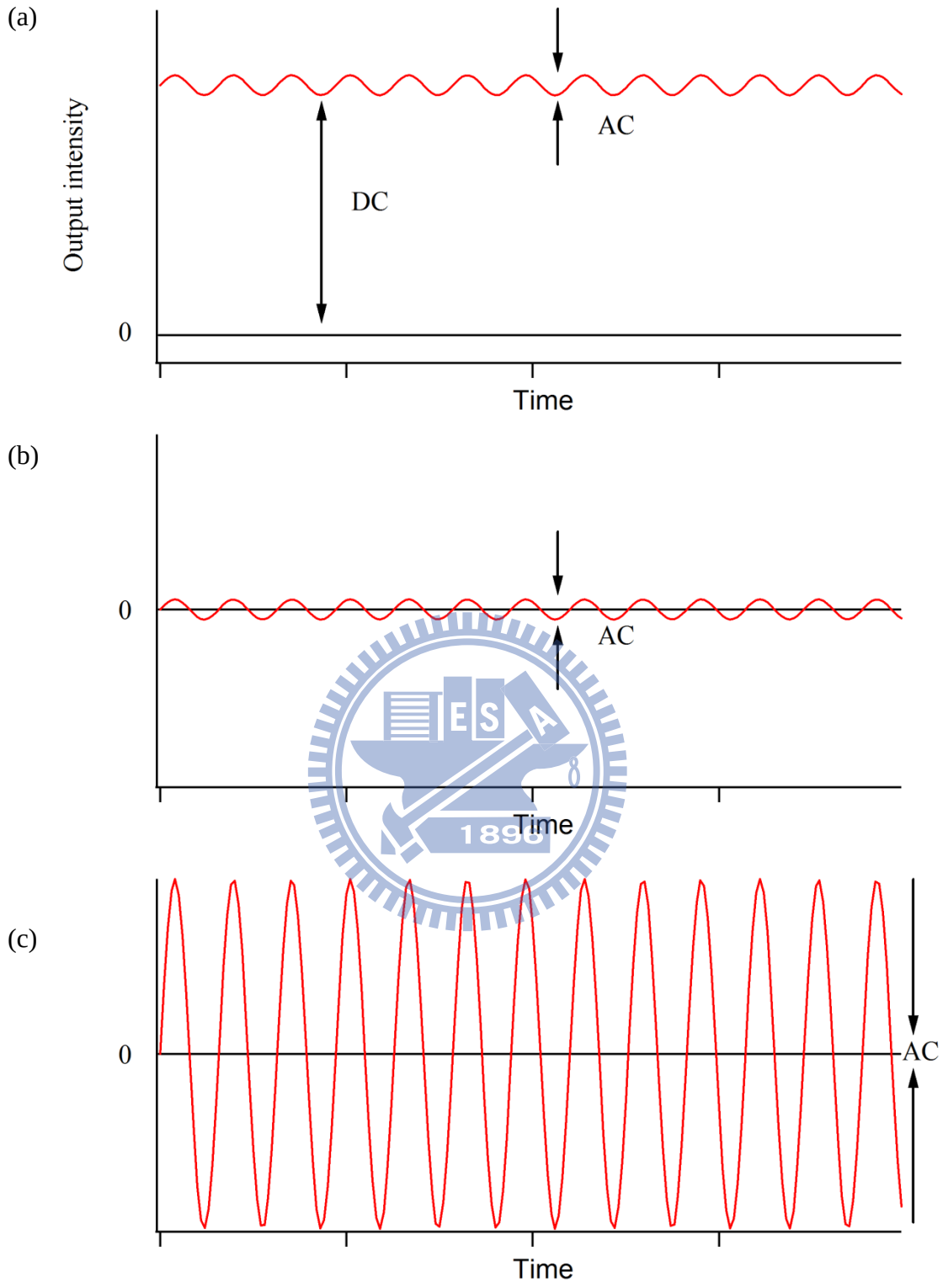

Figure III-2. Schematic of an AC-coupled amplification technique. (a) Output of the detector consisting of a large DC offset and a small AC component. (b) The output is AC-coupled and only the AC component remains. (c) The AC component is then amplified.

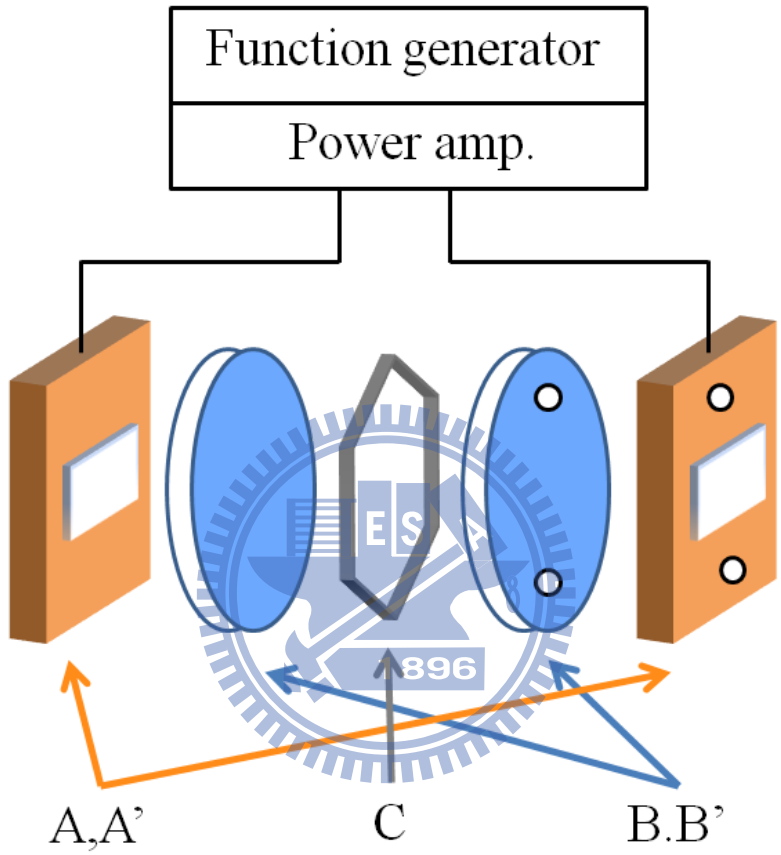

Figure III-3. Configuration of our sample cell. A/A' are brass cell holders, B/B' are Si plates, and C is a PET film used as a spacer.

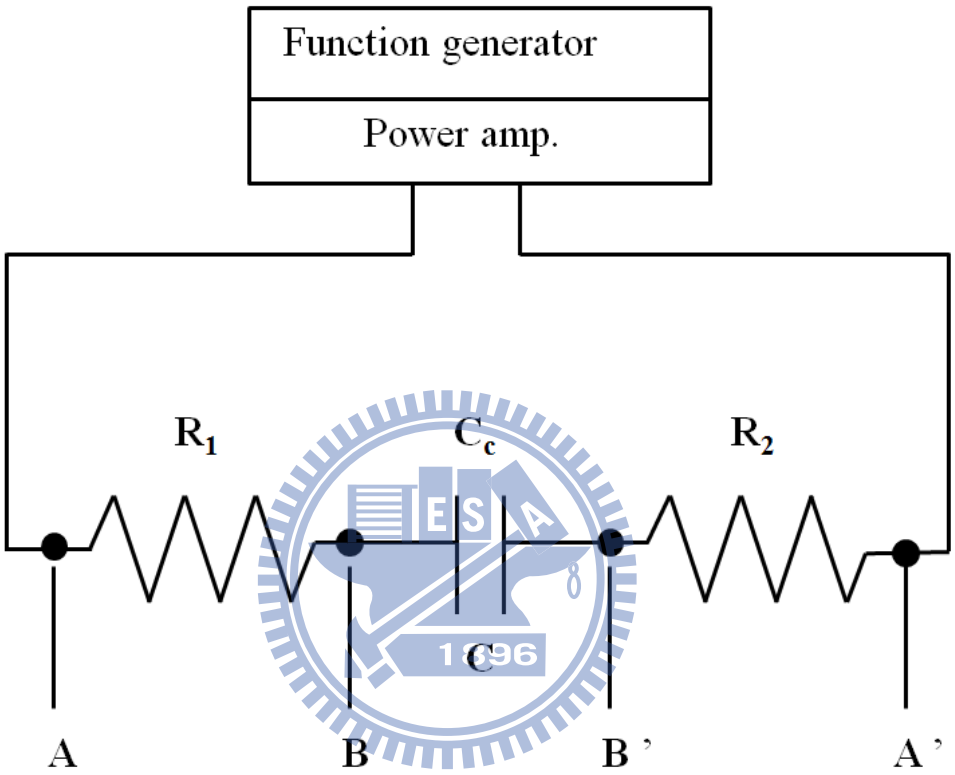

Figure III-4. RC circuit equivalent to the sample cell (Figure III-3.). R_1 is the resistance between A and B, R_2 is that between A’ and B’, and C_C is the capacitance of the capacitor C.

(a)

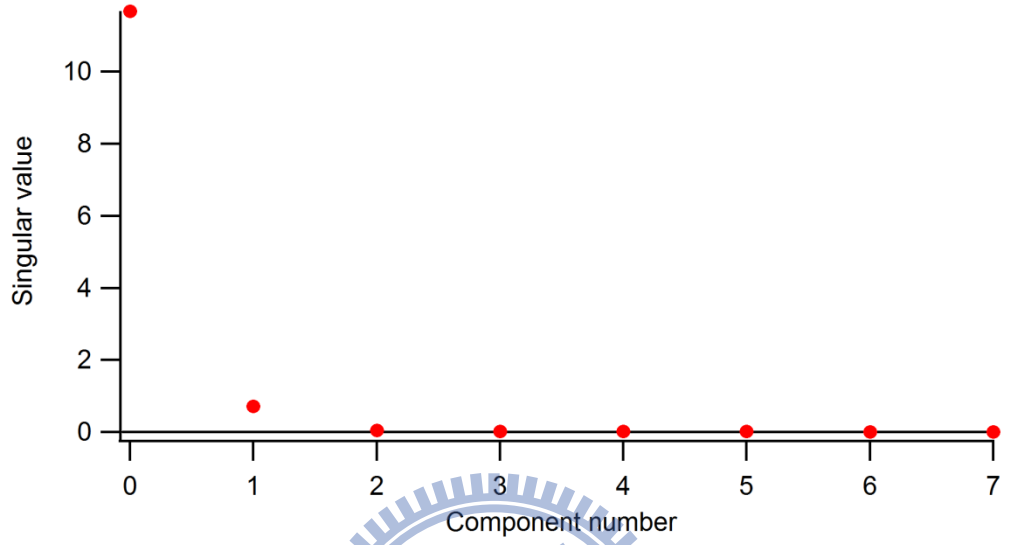

(b)

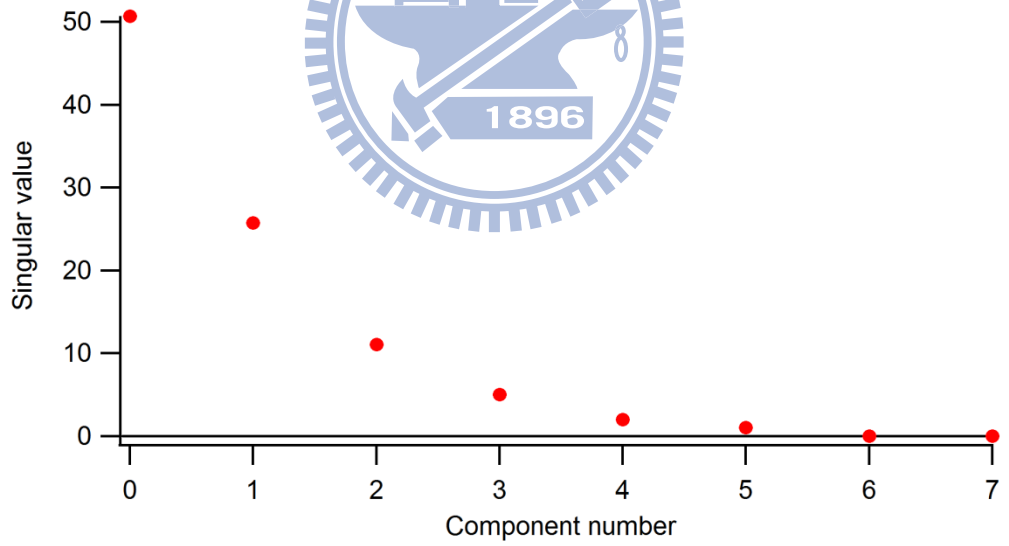

Figure III-5. Plots of singular values typically obtained in singular value decomposition analysis.

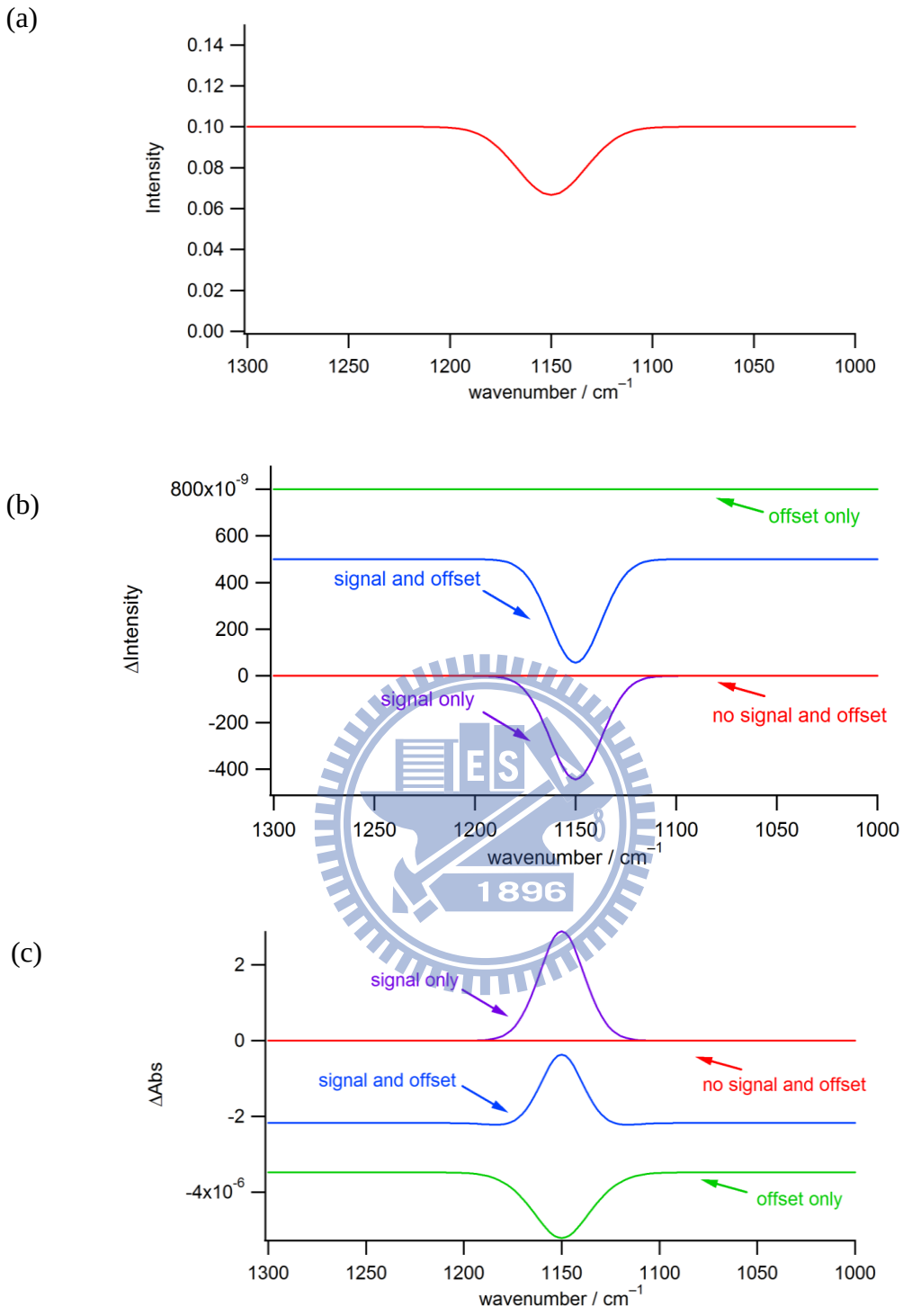

Figure III-6. (a) Intensity spectrum. (b) Δ*I* spectra with neither signal nor offset (red line); with signal only (purple line); with both signal and offset (blue line); and with offset only (green line). (c) Corresponding Δ*A* spectra simulated using Eq. II-1.

Chapter IV

Infrared electroabsorbtion spectroscopic study of water in 1,4-dioxane

IV-1. Introduction

In this chapter, an IR electroabsorption spectroscopic study of water dissolved in 1,4-dioxane is presented. As already described in Chapter I, the O–H stretch [ν(OH)] transition of water occurs as an intense, broad band. Because of the featureless band profile, few clues can be obtained from the steady-state ν(OH) absorption spectrum alone. More insights should be gained by investigating water's responses to an external perturbation, for which we adopt here the application of an external electric field. Since water is polar (μ_P = 2–3 D [36]), it is expected to respond to an externally applied electric field *via* electrostatic interactions.

Although the ultimate goal is the understanding of pure water, there arise several technical difficulties when conducting IR electroabsorption measurements on pure water. Since water has a considerably large dielectric constant ($\varepsilon_r \approx 80$), it causes a significant RC circuit problem described in Chapter III. In addition, the molar extinction coefficient of the ν(OH) band of water is so large that the transmittance in the ν(OH) region can easily fall below the detection limit of the apparatus. A straightforward remedy for this problem would be to make the sample extremely thin, typically thinner than 1 μm [37]. However, it would be inconvenient to employ such a thin sample cell. In this work, we dilute water with solvent. The solvent we used, 1,4-dioxane, is an aprotic solvent with nearly zero dipole moment [36], so the electric-field effects on 1,4-dioxane is expected to be minor.

Water dissolved in 1,4-dioxane, although at a low concentration, is essentially different from pure water. A highly structured network of hydrogen bonding that is present in pure water is lost completely or broken to a great extent in 1,4-dioxane solution. Nevertheless, we believe that it is important as a bottom-up approach to study 1,4-dioxane solution of water, in which water may be thought of as more "free" solute molecules. Such a study can fill a huge gap lying between research for the gas phase and pure liquid. Another important issue relevant

to water in solution is solvation. Solvation is one of the most fundamental phenomena that take place in the solution phase [38-39]. It is an interaction of a solute molecule (water in the present case) with surrounding solvent molecules (1,4-dioxane), which leads to stabilization of the solute molecule in the solution. In a variety of solution-phase chemical reactions, solvation plays an important role in determining the direction and rate of the reactions and in changing the energies of excited as well as the ground state.

First, the concentration dependence of FT-IR absorption spectra of water dissolved in 1,4-dioxane is studied in order to clarify how many water species exist in the solution. The observed concentration-dependent spectra are well-explained by assuming two water species: one is an isolated water molecule interacting solely with 1,4-dioxane, and the other is the water molecule in a small water cluster. Next, the results of IR electroabsorption measurements on the 1,4-dioxane solution of water are shown. As described in Chapter III, the electric resistance of the sample cell often causes artificial phase retardation with respect to the applied sinusoidal wave. Therefore, the phase dependence of the ΔA spectra is examined in order to find the optimum phase for lock-in detection of the signal that can best compensate the phase retardation. The dependence of the ΔA spectra on the field strength F is also studied. We performed an SVD analysis of the ΔA spectra measured at different angles χ and interpreted the results in terms of the two-component model. We find that the orientational polarization contribution to the ΔA spectrum of the ν(OH) band of water is not prominent, whereas the electronic polarization signal originating from $\Delta\boldsymbol{\mu}$, $\Delta\boldsymbol{\alpha}$, and **A** predominates the ΔA spectrum.

IV-2. Experimental section

The experimental apparatus and the sample cell for IR electroabsorption spectroscopy used in this study have already been described in Chapter III. In measuring the angle χ dependence of ΔA spectra, we used a wire-grid mid-IR polarizer to obtain p-polarized light.

Four runs were averaged for each ΔA spectrum, which required about 2 h. The molar concentration of water was 1.0 M for IR electroabsorption measurements.

IV-3. Results and discussion

IV-3-1. Concentration dependence of FT-IR spectra

Figure IV-1(a) shows FT-IR spectra in the 3000–3800 cm^{-1} region of water dissolved in 1,4-dioxane at molar concentrations of 0.25, 0.50, 0.75, 1.0, 1.25, 1.5, 1.75, and 2.0 M. A major broad feature centered at ~3550 cm^{-1}, which apparently consists of two peaks, is observed. This band is unambiguously assigned to the O–H stretch of water. There is a small hump at around 3260 cm^{-1} (see, for example, the 2.0 M spectrum). This band is assigned to the first overtone of the O–H bend, 2δ(OH). The band shape of the ν(OH) band is found to change with water concentration. To better see the change, we normalized the absorption spectra to the intensity at 3514 cm^{-1}. Figure IV-1(b) shows the resulting normalized spectra. As the concentration increases, the higher-wavenumber peak of the ν(OH) band decreases in intensity and concomitantly, the lower-wavenumber side of the band appears to be broadened.

We also measured the concentration dependence of FT-IR spectra of water in 1,4-dioxane at lower concentrations of 0.05, 0.10, 0.15, 0.20, 0.25, 0.30, 0.35, and 0.40 M. Figure IV-2(a), (b) shows the raw data and the spectra normalized to the intensity at 3514 cm^{-1}, respectively. As can be seen from Fig. IV-2(a), the band shape of the ν_{OH} band and the intensity ratio of its two peaks look similar in this concentration range. However, the normalized spectra shown in Fig. IV-2(b) do exhibit the same tendency as in Fig. IV-1(b), although somewhat less prominent. These results seem to indicate that the water species responsible for the observed ν(OH) band may exist even at low concentrations (<0.40 M).

In order to know how many water species are involved in the 1,4-dioxane solution in the concentration range studied, we analyzed the spectra using multivariate curve resolution

(MCR). In MCR analysis, a data matrix **X** consisting of a series of spectra at different concentrations is decomposed into physically meaningful matrices **H** and **W**. The matrix **H** contains normalized concentration profiles of individual molecular components and the matrix **W** contains the corresponding intrinsic spectra. The sum squared residual $\left\|\mathbf{X}-\mathbf{H}\mathbf{W}^{\mathrm{T}}\right\|$ is minimized by solving alternating least-squares problems iteratively under the constraint that concentration and spectral intensity (*i.e.*, the matrix elements of **H** and **W**) are non-negative. In MCR analysis, we need to assume the number of components *a priori*. Here, we refer to the result of SVD of the dataset shown in Fig. IV-1(a). Figure IV-3 plots the singular values obtained from the SVD. It is clear that there are two principal singular values. We therefore set the number of components required in MCR as two. Hereafter the major component will be denoted 1 and the minor 2. A randomly generated basis was used as an initial guess for **W**. 1000 iterations were enough to obtain a good convergence regardless of the initial guess.

What molecular models can be applied to account for the water components 1 and 2? Since the major component 1 exists even at low concentrations, it would be natural to attribute it to an isolated water molecule surrounded by 1,4-dioxane molecules as depicted in Fig. IV-4(a). On the other hand, we hypothesize that the minor component 2 is assigned to water species inside a small cluster (ensemble) of water molecules that forms hydrogen bonds with neighboring water molecules or 1,4-dioxane molecules outside the cluster [Fig. IV-4(b)].

The concentration profiles ($\mathbf{h}_1$ and $\mathbf{h}_2$) and intrinsic spectra ($\mathbf{w}_1$ and $\mathbf{w}_2$) of components 1 and 2 derived from the MCR analysis are displayed in Fig. IV-5. As expected, the $\mathbf{w}_1$ spectrum explains the major feature of the O–H stretch band of water, in which two peaks at around 3600 and 3500 cm^{-1} are dominant. The two peaks are reminiscent of the antisymmetric and symmetric O–H stretches, ν_{as}(OH) and ν_s(OH), of water. It is not surprising that the $\mathbf{w}_1$ spectrum shows two distinct ν(OH) peaks in contrast with the broad,

featureless ν(OH) band of pure liquid water, because component 1 has been considered in our model as an isolated water molecule in the 1,4-dioxane medium. In this sense, the $\mathbf{w}_1$ spectrum is consistent with our model of water. We fit the $\mathbf{w}_1$ spectrum to a sum of three Lorentzian functions plus a baseline represented by a linear function. The two Lorentzian functions at higher wavenumbers account for the ν_{as}(OH) and ν_s(OH) bands, and the third one with very small intensity for the first overtone of δ(OH). The best fit is shown in Fig. IV-6(a), and the peak positions and band widths of the three bands are given in Table 1.

The $\mathbf{w}_2$ spectrum shows a more complicated band profile, which has a maximum at a lower wavenumber relative to the $\mathbf{w}_1$ spectrum and includes at least three peaks. The profile of the $\mathbf{w}_2$ spectrum resembles the inhomogeneously broadened ν(OH) band of pure water. This similarity in spectral profile is consistent with our model for component 2, in which the component is assigned to a water molecule in a water cluster. In fact, the $\mathbf{w}_2$ spectrum can be well reproduced by a sum of two Gaussian functions and one Lorentzian function (plus a baseline) rather than a sum of three Lorentzian functions, implying inhomogeneous characteristics of the $\mathbf{w}_2$ spectrum. The best fit is shown in Fig. IV-6(b), and the peak positions and band widths of the three bands are given in Table 2.

IV-3-2. Phase dependence of IR electroabsorption spectra

As described in Chapter III, a large resistance of the sample cell may give rise to a decrease in amplitude of the applied voltage and phase retardation with respect to the applied sinusoidal wave. The latter may result in nonzero out-of-phase Δ*A* signals. In this section, we show the dependence of Δ*A* spectra on lock-in detection phase. The Δ*A* spectrum was measured at four different phases: −90°, −100°, −110°, and −120°. In our setting, if the sample cell is an ideal capacitor with zero resistance, there will be no out-of-phase Δ*A* signal at −90°. A 25 kHz sinusoidal wave of an electric field whose amplitude was ~1.2 × 10^7 V m^{-1} was applied across the cell gap of about 6 μm. The in-phase and out-of-phase Δ*A* spectra are shown

in Fig. IV-7(a), (b), respectively. The in-phase Δ*A* spectrum is less affected by changing the detection phase; only a small variation in signal amplitude can be seen. In the out-of-phase Δ*A* spectrum, however, the feature at ~3550 cm^{-1} swings from a negative dip at −90° to a positive signal at −120°. We believe that the observed out-of-phase Δ*A* signal is not of molecular origin but artifacts produced electrically. At −110°, the out-of-phase signal at ~3550 cm^{-1} is effectively removed, so we chose to measure all the Δ*A* spectra presented below at this detection phase.

Regardless of the detection phase, the Δ*A* spectra shown in Fig. IV-7(a) all have a negative offset of about 5×10^{-7}. To eliminate this offset, we subtracted the Δ*A* spectrum recorded under the same conditions but without electric field [gray line in Fig. IV-8(a)]. Nonzero signals in the $F = 0$ spectrum may be due to some electrical artifacts. Subtraction of the $F = 0$ spectrum also removes a negative signal at ~3750 cm^{-1}, which is caused presumably by the artifact illustrated in Fig. III-6. The resulting Δ*A* spectrum still has a slowly varying baseline [Fig. IV-8(b)], which was fit to a sine function and then subtracted off from the Δ*A* spectrum. After these corrections, the Δ*A* spectrum shows a flat baseline fluctuating around $\Delta A = 0$. The Δ*A* spectra presented hereafter have been subjected, if necessary, to the above-mentioned baseline corrections.

IV-3-3. Electric field strength dependence of IR electroabsorption spectra

Figure IV-9(a) shows the Δ*A* spectra in the ν(OH) region of water dissolved in 1,4-dioxane obtained with applied voltages ($V_{0\text{-}p}$) of 50, 70, and 80 V. These voltages are equal to the strength of the external electric field of 8.3, 11.7, and 13.3 MV m^{-1}, respectively. As the field strength *F* increases, the Δ*A* signal of water gets stronger with the spectral shape unchanged. As discussed in Chapter II (see Eq. II-24), Δ*A* signals observed in our experiment are expected to be proportional to the square of the field strength *F*. Figure IV-9(b) plots the Δ*A* signals integrated for the 3516–3572 and 3580–3684 cm^{-1} intervals as a function the square of

the field strength, F^2. It is found that that both positive (3516–3572 cm^{-1}) and negative (3580–3684 cm^{-1}) ΔA signals are proportional to F^2, ensuring that what we detect here is the second-order Stark effect.

IV-3-4. Angle χ dependence of IR electroabsorption spectra

Figure IV-10(a) shows the ΔA spectra in the ν(OH) region of water in 1,4-dioxane (1.0 M, $F_{ext} = 1.17 \times 10^7$ V m^{-1}) at five different angles χ = 55°, 63°, 72°, 81°, and 90°. ΔA signal in the O–H stretch region as small as 1×10^{-6} has been successfully detected for the first time. At χ = 90° (normal incidence of the IR light to the sample cell), the ν(OH) ΔA spectrum is predominated by a positive peak centered at ~3540 cm^{-1} and a broad dent between 3600 and 3700 cm^{-1}. As χ varies from 90° to 55° (magic angle), the positive peak gradually diminishes, but the negative peak remain almost unchanged. To examine the number of independent components involved in the observed χ dependence, we performed SVD of the data. The singular values obtained from the SVD are plotted in Fig. IV-10(b), in which at least two major components are found. With singular values alone, it is difficult to determine whether or not the third and later components should be taken into account in subsequent analysis. Referring to the intrinsic spectra of the largest four components [Fig. IV-10(c)], we find that the spectra of the third and fourth components contain only noises with no appreciable vibrational features in the ν(OH) region. Therefore, we will focus on the largest two components and disregard the remaining components as noises (see Eq. III-13). Like in previous studies [16, 18], we assume that the surviving two singular values are associated with a χ-independent (constant with respect to χ) component and a χ-dependent component which behaves as $1-3\cos^2\chi$. By taking a proper linear combination of the vectors (recall Eqs. III-14 and III-15) based on the model for χ dependence, we can obtain physically meaningful vectors. The reconstructed χ dependence and spectra are shown in Fig. IV-11(a), (b), respectively. As shown in Fig. IV-12(a), the reconstructed ΔA spectra are overall in good agreement with the

observed spectra.

The χ-dependent component spectrum [blue spectrum in Fig. IV-11(b)] is dominated by a positive peak centered at ~3540 cm^{-1} with no appreciable negative dip in other regions. Because the χ-dependent component vanishes at around χ = 55°, the χ-independent component spectrum [red spectrum in Fig. IV-11(b)] is almost identical to the χ = 55° spectrum. It is composed of two negative bands: the larger feature is located at ~3600 cm^{-1}, and the smaller one appears around 3500 cm^{-1}.

IV-3-5. Fitted results of the χ-independent and χ-dependent component spectra

In this section, we fit the χ-independent and χ-dependent component spectra to Eq. II-24 using the $\mathbf{w}_1$ spectrum composed of two distinct water species determined by the MCR analysis. The concentration-weighted IR spectra of components 1 and 2 (total water concentration = 1.0 M) are shown in Fig. IV-13(a). The peak height of the $\mathbf{w}_2$ spectrum is about four times weaker than that of the two Lorentzian bands consisting of the $\mathbf{w}_1$ spectrum. As a result, the contribution of component 2 to the ΔA spectra is anticipated to be comparable to the noise level ($<0.5 \times 10^{-6}$). Here we thus make a bit crude approximation that it is neglected in the fitting analysis of the ΔA spectra and only component 1 (*i.e.* antisymmetric and symmetric stretch bands of isolated water) is taken into account.

In the fitting, the band widths and peak positions of the ν_{as}(OH) and ν_s(OH) bands are fixed to the values tabulated in Table IV-1. Under these conditions, the χ-independent and χ-dependent component spectra were fit to a linear combination of the zeroth, first, and second derivatives of each absorption band (Lorentzian). The results for the χ-independent and χ-dependent spectra are shown in Fig. IV-13(b), (c) and Fig. IV-14(b), (c), respectively. The parameters, a_χ, b_χ, and c_χ, for each band determined by the fitting are summarized in Table 3. They are related to the coefficients, A_χ, B_χ, and C_χ, in Eq. II-24 *via* the following equations:

$$a_\chi = F^2 A_\chi \qquad \text{(IV-1)}$$

$$b_\chi = \frac{F^2}{15hc} B_\chi = \left(3.356\times10^{23} F^2\right) B_\chi \qquad \text{(IV-2)}$$

$$c_\chi = \frac{F^2}{30h^2c^2} C_\chi = \left(8.447\times10^{47}\right) F^2 C_\chi \qquad \text{(IV-3)}$$

Some of the coefficients [*e.g.*, a_χ for the ν_{as}(OH) band in the χ-dependent ΔA spectrum] turned out not to affect the fit, so they were set equal to zero in the spirit of reducing the number of adjustable parameters. In addition, during the fitting, we imposed a relation between the c_χ's for ν_s(OH) of the χ-independent and χ-dependent components, as requested by Eq. II-27 (*vide infra*).

Figures IV-13(c) and IV-14(c) reveal the following qualitative features. (1) The χ-independent spectrum is dominated by the zeroth and second derivative components. Within experimental errors, we conclude that there is no contribution from the first derivative term. Because the ν_{as}(OH) and ν_s(OH) bands are vibrational modes of the same molecule, an equilibrium shift cannot contribute to the zeroth derivative component in the present case. Therefore, the result seems to suggest a significant contribution of the transition polarizability **A**. (2) The χ-dependent spectrum has contributions from all the three terms with the first derivative term being dominant. (3) In the χ-dependent spectrum, the zeroth derivative signal of ν_{as}(OH) is zero and that of ν_s(OH) is positive. This is quite surprising because the ν_{as}(OH) mode (α = 90°) and ν_s(OH) mode (α = 0°) should give positive and negative ΔA signals, respectively, if orientational polarization is the main contributor as is often the case [29]. Again, the fitted result is indicative of large contributions of the transition polarizability **A**. (4) The second derivative term, which is proportional to $|\Delta\boldsymbol{\mu}|^2$, is zero for the ν_{as}(OH) band but nonzero for the ν_s(OH) band. This can be rationalized in a qualitative manner as follows. The transition moment **m** is perpendicular to $\boldsymbol{\mu}_g$ for ν_{as}(OH), so the $v = 1 \leftarrow 0$ excitation does not

alter the dipole moment much, resulting in $\boldsymbol{\mu}_e \approx \boldsymbol{\mu}_g$ and hence $|\Delta\boldsymbol{\mu}| \approx 0$. On the other hand, the transition moment of the ν_s(OH) mode is parallel to $\boldsymbol{\mu}_g$, so the vibrational excitation of this mode would induce a significant change in dipole moment, resulting in $\boldsymbol{\mu}_e \neq \boldsymbol{\mu}_g$ and hence $|\Delta\boldsymbol{\mu}| \neq 0$.

From the parameters a_χ, b_χ, and c_χ, the values of the molecular properties such as $\Delta\boldsymbol{\alpha}$, $\Delta\boldsymbol{\mu}$, and **A** can, in principle, be obtained using Eqs. II-25–27, although it is often necessary to make further assumptions or simplifications (*e.g.*, **A** is a symmetric tensor). Equations II-25–27 can be divided into two parts according to dependence on angle χ. The fragments that show the $3\cos^2\chi - 1$ dependence are

$$\begin{aligned} A_{3\cos^2\chi-1} = {} & \frac{1}{30|\mathbf{m}|^2}\sum_{ij}\left(3A_{ii}A_{jj} + 3A_{ij}A_{ji} - 2A_{ij}^2\right)\left(3\cos^2\chi - 1\right) \\ & + \frac{1}{15|\mathbf{m}|^2 k_B T}\sum_{ij}\left(3m_i A_{ji}\mu_{gj} + 3m_i A_{jj}\mu_{gi} - 2m_i A_{ij}\mu_{gj}\right)\left(3\cos^2\chi - 1\right) \\ & + \frac{1}{10k_B T}\left(\alpha_{gm} - \overline{\alpha_g}\right)\left(3\cos^2\chi - 1\right) + \frac{\mu_g^2}{30k_B^2 T^2}\left(3\cos^2\alpha - 1\right)\left(3\cos^2\chi - 1\right) \end{aligned} \quad \text{(IV-4)}$$

$$\begin{aligned} B_{3\cos^2\chi-1} = {} & \frac{1}{|\mathbf{m}|^2}\sum_{ij}\left(3m_i A_{ji}\Delta\mu_j + 3m_i A_{jj}\Delta\mu_i - 2m_i A_{ij}\Delta\mu_j\right)\left(3\cos^2\chi - 1\right) \\ & + \frac{3}{2}\left(\Delta\alpha_m - \overline{\Delta\alpha}\right)\left(3\cos^2\chi - 1\right) \\ & + \frac{1}{k_B T}\left[3\left(\hat{\mathbf{m}}\cdot\boldsymbol{\mu}_g\right)\left(\hat{\mathbf{m}}\cdot\Delta\boldsymbol{\mu}\right) - \left(\boldsymbol{\mu}_g\cdot\Delta\boldsymbol{\mu}\right)\right]\left(3\cos^2\chi - 1\right) \end{aligned} \quad \text{(IV-5)}$$

$$C_{3\cos^2\chi-1} = \left[3\left(\hat{\mathbf{m}}\cdot\Delta\boldsymbol{\mu}\right) - |\Delta\boldsymbol{\mu}|^2\right]\left(3\cos^2\chi - 1\right) \quad \text{(IV-6)}$$

The -independent terms are

$$A_{const} = \frac{1}{30|\mathbf{m}|^2}\sum_{ij}10A_{ij}^2 + \frac{1}{15|\mathbf{m}|^2 k_B T}\sum_{ij}10m_i A_{ij}\mu_{gj} \quad \text{(IV-7)}$$

$$B_{\text{const}} = \frac{1}{|\mathbf{m}|^2}\sum_{ij} m_i A_{ij} \Delta\mu_j + \frac{15}{2}\overline{\Delta\alpha} + \frac{5}{k_B T}\left(\boldsymbol{\mu}_g \cdot \Delta\boldsymbol{\mu}\right) \qquad \text{(IV-8)}$$

$$C_{\text{const}} = 5\left|\Delta\boldsymbol{\mu}\right|^2 \qquad \text{(IV-9)}$$

It follows from Eqs. IV-6 and IV-9 that $C_{3\cos^2\chi-1}$ and C_{const} cannot be independent. Assuming that $\Delta\boldsymbol{\mu}$ is parallel to $\boldsymbol{\mu}_g$, $3\left(\hat{\mathbf{m}}\cdot\Delta\boldsymbol{\mu}\right)-\left|\Delta\boldsymbol{\mu}\right|^2 = \left|\Delta\boldsymbol{\mu}\right|^2(3\cos^2\alpha-1)$, where α is the angle between the transition moment and the ground-state dipole moment. Therefore, the constraint between $C_{3\cos^2\chi-1}$ and C_{const} is found to be

$$\frac{C_{3\cos^2\chi-1}}{C_{\text{const}}} = \frac{1}{5}(3\cos^2\alpha-1)(3\cos^2\chi-1) = -\frac{2}{5}(1-3\cos^2\chi) \qquad \text{(IV-10)}$$

Here we used α = 0°. In the actual fitting, the χ-independent component spectrum [Fig. IV-13(b)] was fit first, yielding the value of c_χ for the ν_s(OH) band, 4.22 × 10^{-3}. The fit was not good if we did not the second derivative component. Using the relation Eq. IV-10, the value of c_χ for the ν_s(OH) band in the χ-dependent component spectrum was obtained as −1.69 × 10^{-3}, which was fixed during the fitting of the χ-dependent spectrum.

Using Eqs. IV-3 and IV-9, $|\Delta\boldsymbol{\mu}|$ is evaluated to be 8.1 × 10^{-4} D/f. Here $f = f' \cdot f''$ (recall Eqs. III-7 and III-8). The local-field correction f'' is larger than unity, but in our experiment, a voltage drop (f') is much smaller than unity. As a result, the product f is usually smaller than unity. For example, it was found to be about 0.6 in the previous work [23, 27]. Taking the factor f into account, the value of $|\Delta\boldsymbol{\mu}|$ is of the order of 10^{-3} D. Andrews and Boxer [21] reported the values of $|\Delta\boldsymbol{\mu}|$ for the C≡N stretch modes of nitrile compounds embedded in frozen glass matrix, all of which are of the order of 10^{-2} D. The $|\Delta\boldsymbol{\mu}|$ value that we have obtained for the ν_s(OH) mode of water is one order of magnitude smaller than that for the C≡N stretch.

It will also be possible to evaluate $\overline{\Delta\alpha}$ and the tensor elements of **A** using Eqs. IV-7 and IV-8. However, the signal-to-noise ratio in our experiment is still not high enough to enable us to determine these quantities accurately. Improvement in data quality and more detailed quantitative analysis are left for the future studies.

Table 1. Peak positions and band widths determined from the fitting of the $\mathbf{w}_1$ spectrum [Fig. IV-6(a)].

	Peak position (cm^{-1})	Band width (cm^{-1})
Lorentzian 1	3589	84
Lorentzian 2	3507	99
Lorentzian 3	3262	80

Table 2. Peak positions and band widths determined from the fitting of the $\mathbf{w}_2$ spectrum [Fig. IV-6(b)].

	Peak position (cm^{-1})	Band width (cm^{-1})
Lorentzian 1	3545	49
Gaussian 1	3456	138
Gaussian 2	3323	231

Table 3. The fitted parameters a_χ, b_χ, and c_χ, of the zeroth, first, and second derivative terms of the χ-dependent and χ-independent ΔA spectra of water in 1,4-dioxane.

	χ-independent ΔA spectrum		χ-dependent ΔA spectrum	
	ν_{as}(OH)	ν_s(OH)	ν_{as}(OH)	ν_s(OH)
a_χ	-4.7×10^{-6}	2.52×10^{-6}	0	1.92×10^{-6}
b_χ	0	0	6.69×10^{-5}	1.87×10^{-4}
c_χ [a]	0	4.22×10^{-3}	0	-1.69×10^{-3}

[a] The parameters for the χ-independent and χ-dependent component spectra are related to each other by Eq. IV-10.

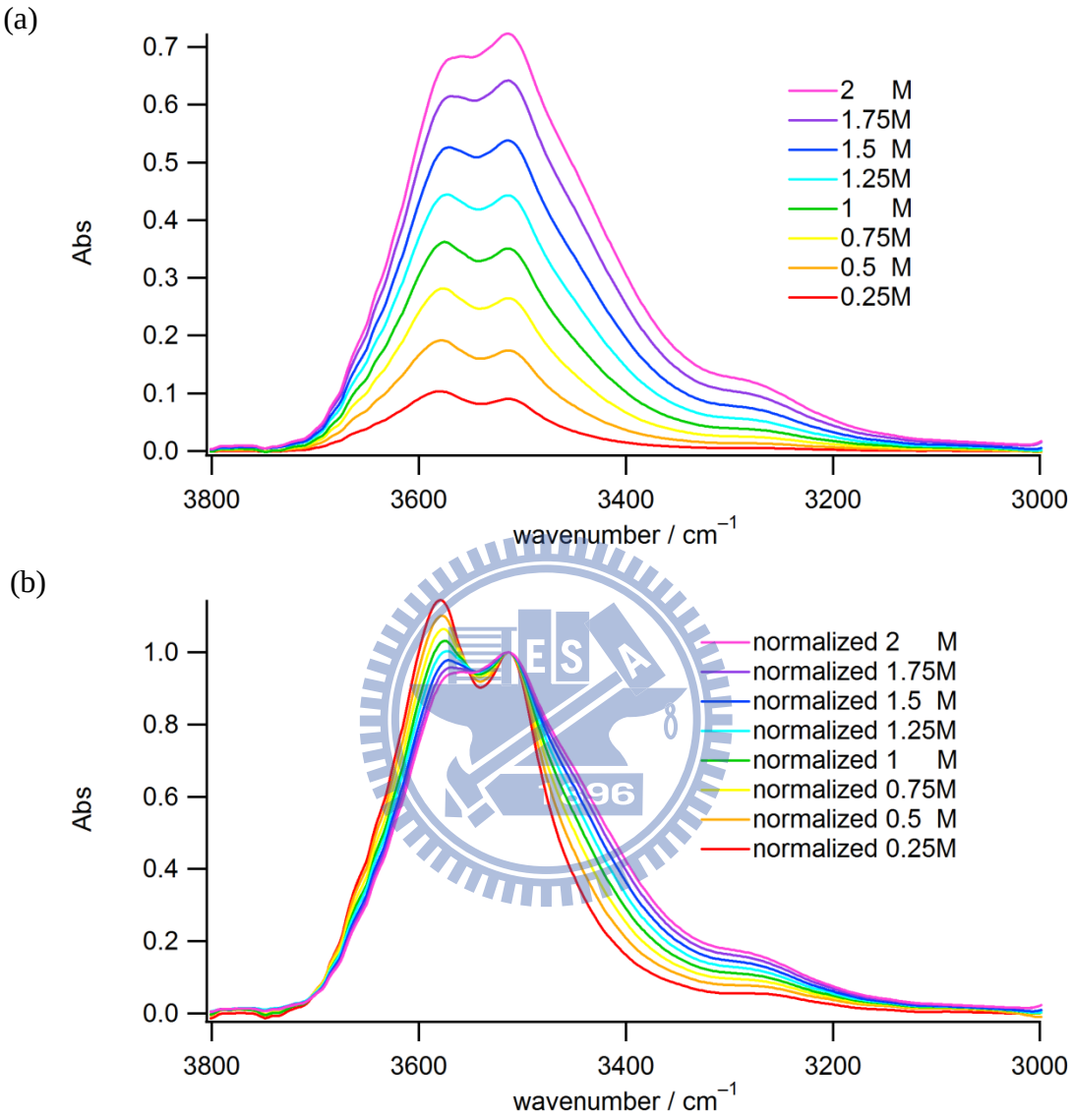

Figure IV-1. (a) Concentration dependence of FT-IR spectra in the 3000–3800 cm^{-1} region, of water dissolved in 1,4-dioxane at eight different concentrations. (b) The same spectra as in part (a) but normalized to the intensity at 3514 cm^{-1}.

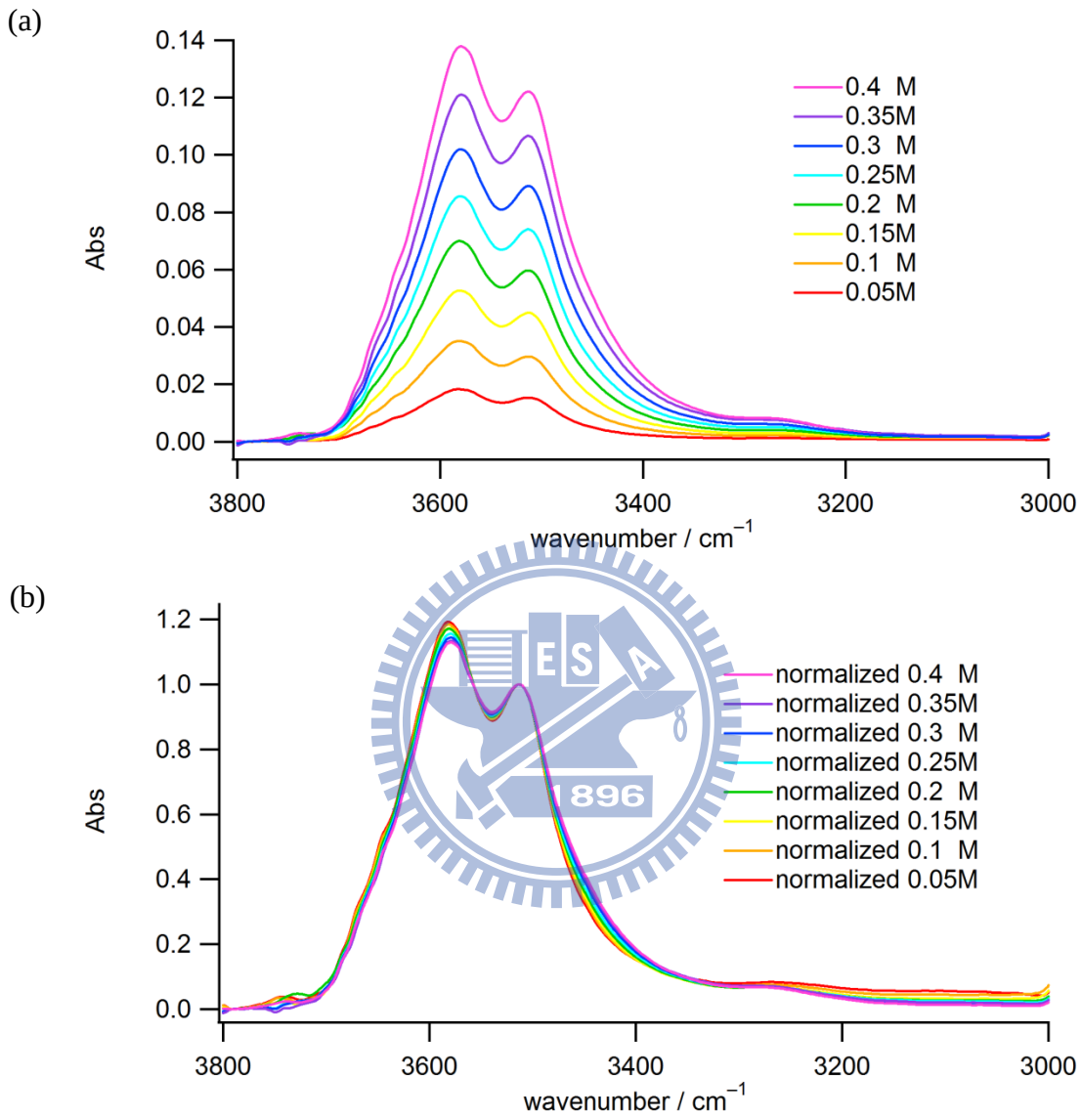

Figure IV-2. (a) Concentration dependence of FT-IR spectra in the 3000–3800 cm^{-1} region, of water dissolved in 1,4-dioxane at eight different concentrations below 0.4 M. (b) The same spectra as in part (a) but normalized to the intensity at 3514 cm^{-1}.

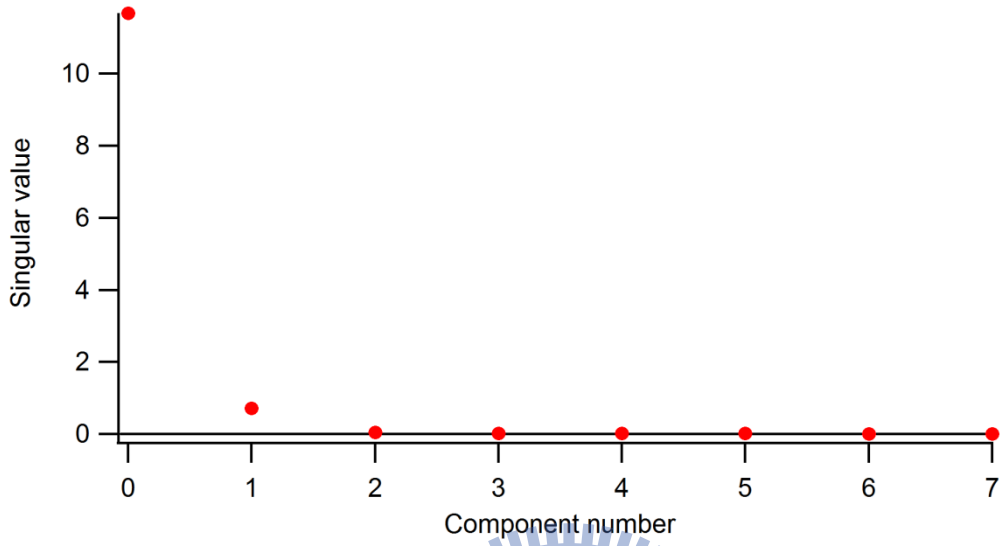

Figure IV-3. Plot of singular values obtained by the SVD of the FT-IR spectra at different concentrations (Fig. IV-1(a)). Two principal singular values have been yielded.

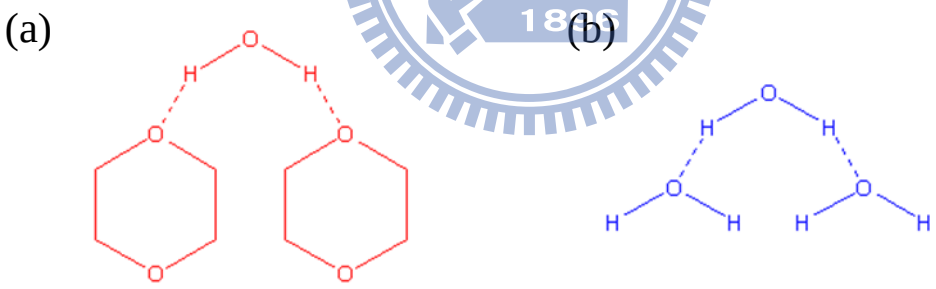

Figure IV-4. Models for the water components 1 and 2. (a) The major component 1 is an isolated water molecule surrounded by 1,4-dioxane molecules. (b) The minor component 2 is a water molecule inside a small cluster (ensemble) of water. This water molecule forms hydrogen bonds with neighboring water molecules in the ensemble and/or 1,4-dioxane.

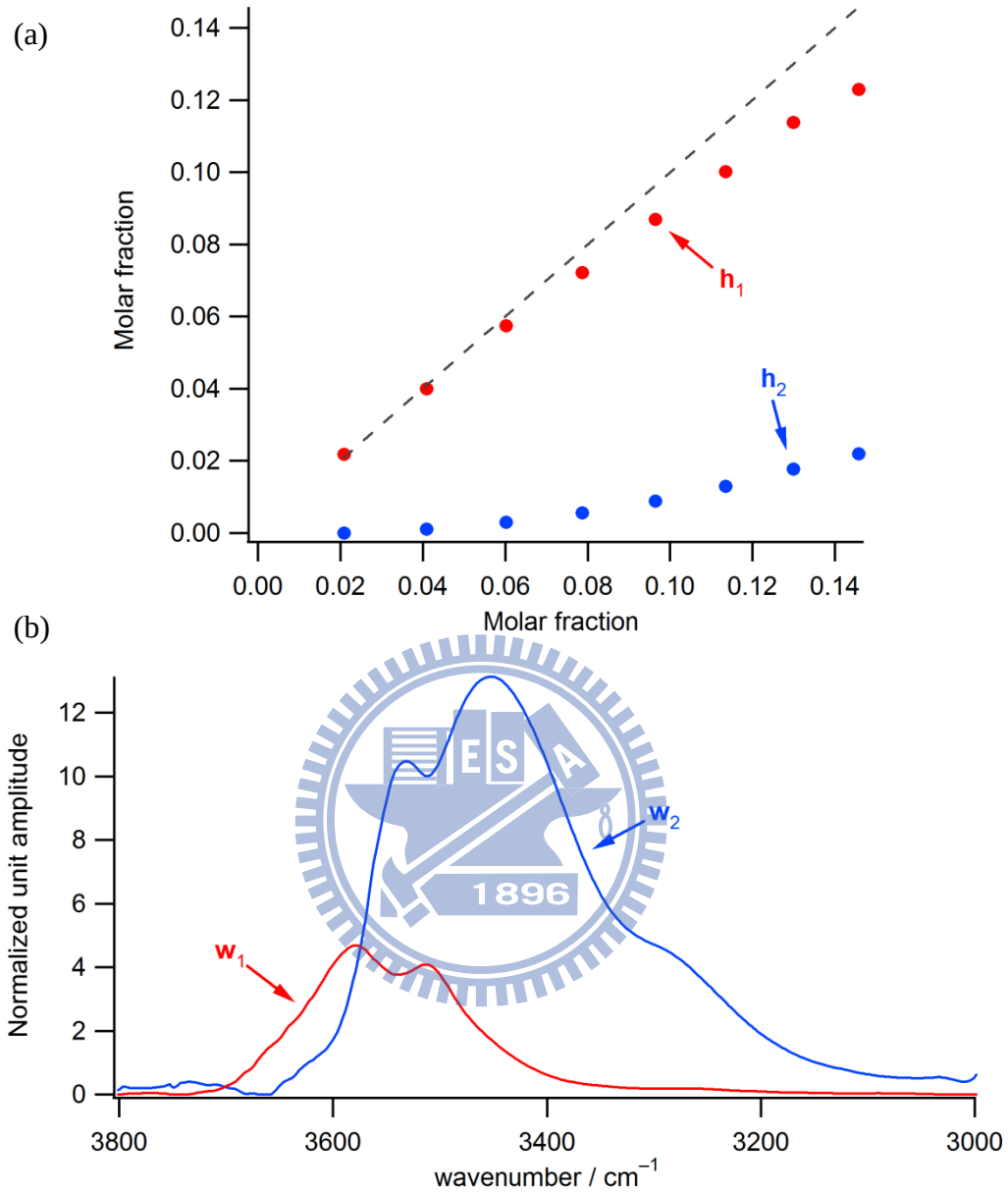

Figure IV-5. The results of MCR analysis under the assumption that there are two water components present in 1,4-dioxane solution. (a) Mole fraction profiles ($\mathbf{h}_1$ and $\mathbf{h}_2$). The dashed line represents the sum of $\mathbf{h}_1$ and $\mathbf{h}_2$. (b) Intrinsic spectra ($\mathbf{w}_1$ and $\mathbf{w}_2$).

(a)

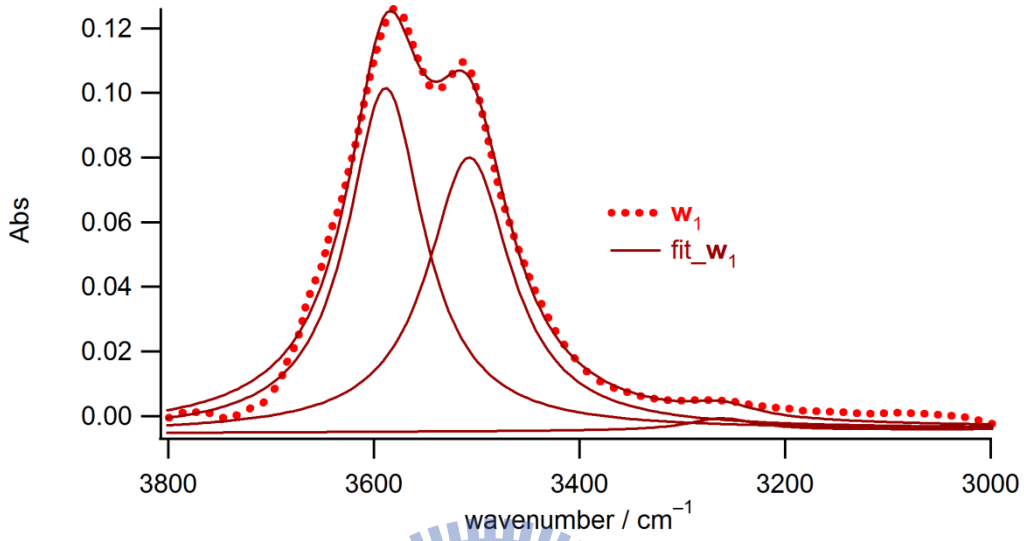

(b)

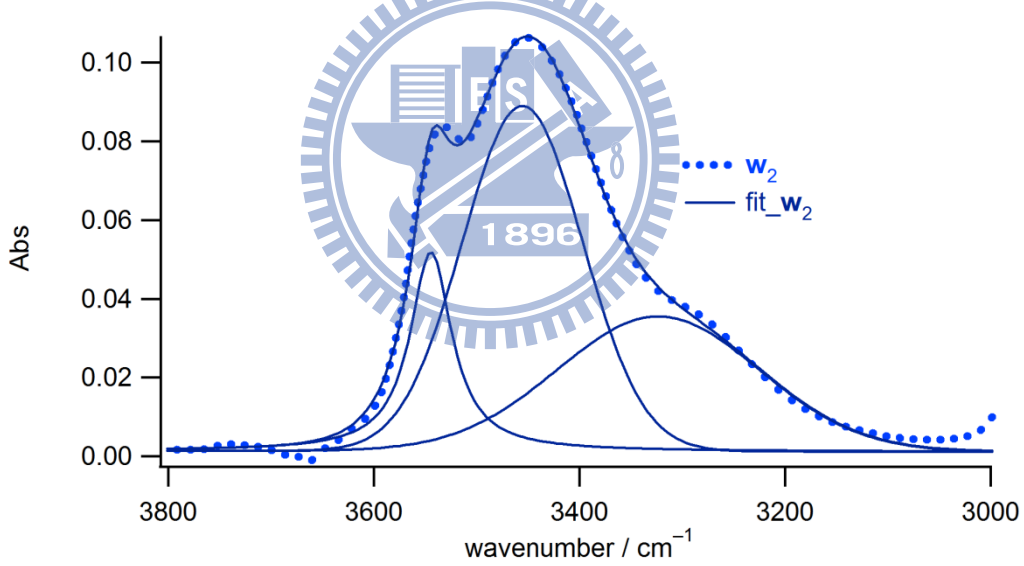

Figure IV-6. (a) Fit of the $\mathbf{w}_1$ spectrum to a sum of three Lorentzian functions plus a baseline represented by a linear function. (b) Fit of the $\mathbf{w}_2$ spectrum to a sum of one Lorentzian function and two Gaussian functions plus a baseline represented by a linear function. In both (a) and (b), the dotted line is the spectrum derived from MCR, and the solid lines are the overall fit and Lorentzian/Gaussian band for each component.

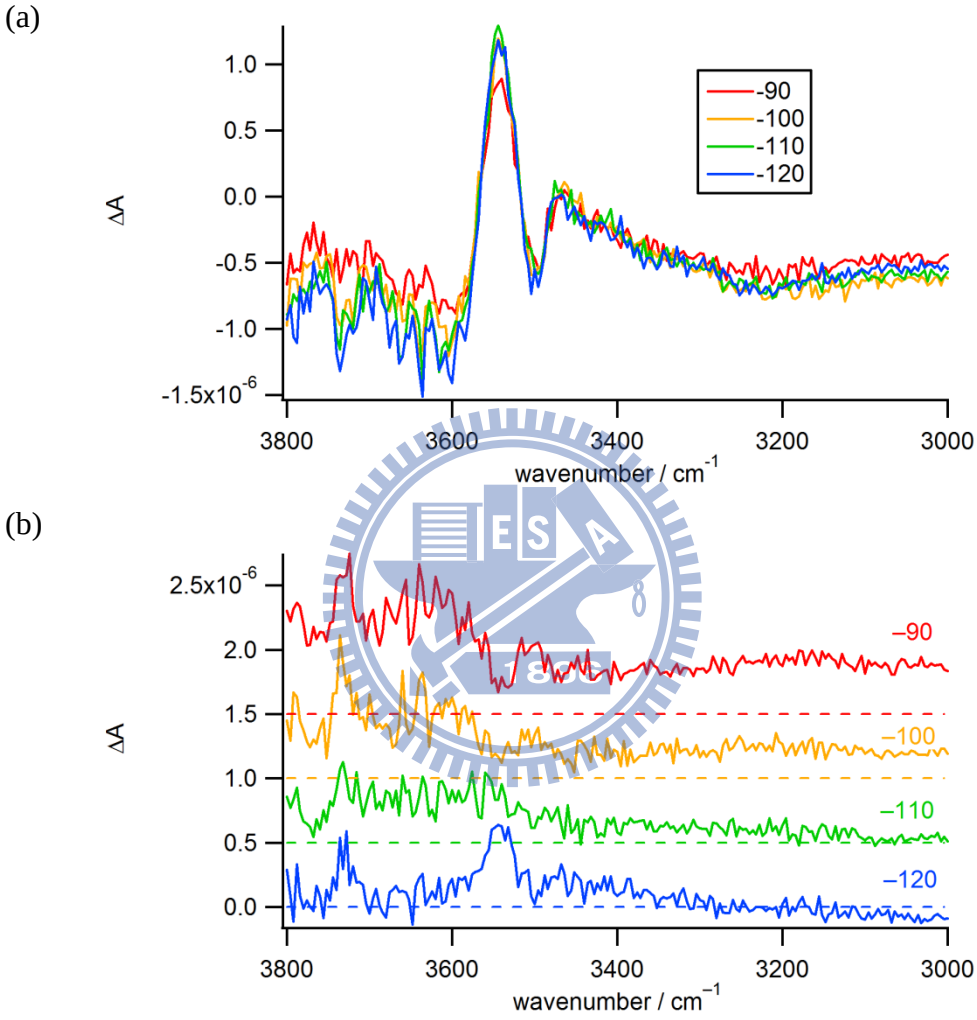

Figure IV-7. (a) In-phase Δ*A* spectra recorded at four different lock-in detection phases (−90°, −100°, −110°, and −120°) and (b) the corresponding out-of-phase Δ*A* spectra. Each out-of-phase Δ*A* spectrum is offset by 0.5×10^{-6} for clarity of presentation. The sample was water in 1,4-dioxane (1.0 M).

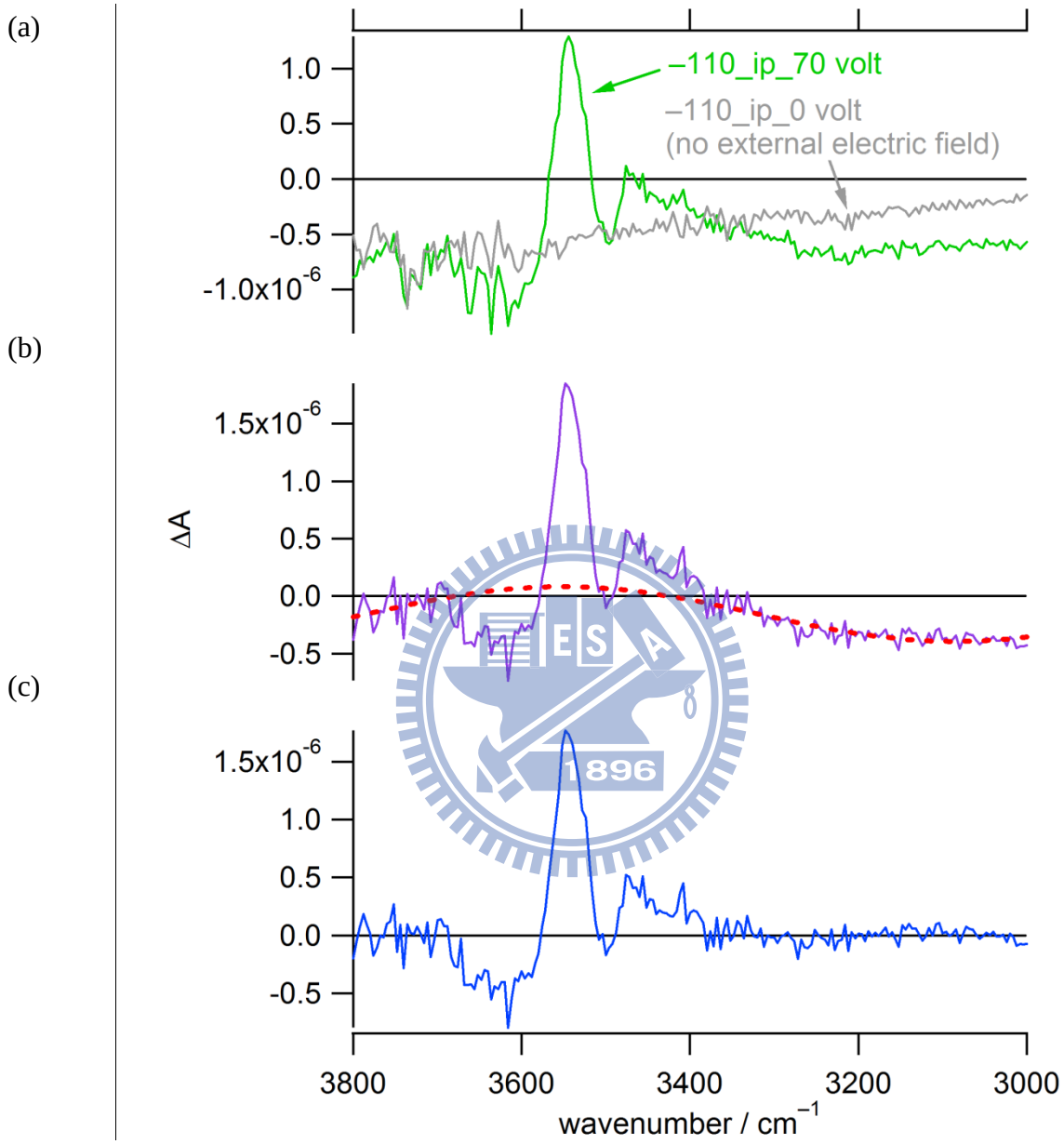

Figure IV-8. Illustration of baseline corrections for the typical Δ*A* spectrum of water in 1,4-dioxane (1.0 M). (a) The Δ*A* spectrum without any electric field applied (gray line) is subtracted off from the Δ*A* spectrum with electric field turned on (green line). (b) A slowly varying baseline is fit to a sine function (red dotted line) and subtracted further from the Δ*A* spectrum. (c) The final Δ*A* spectrum after the corrections.

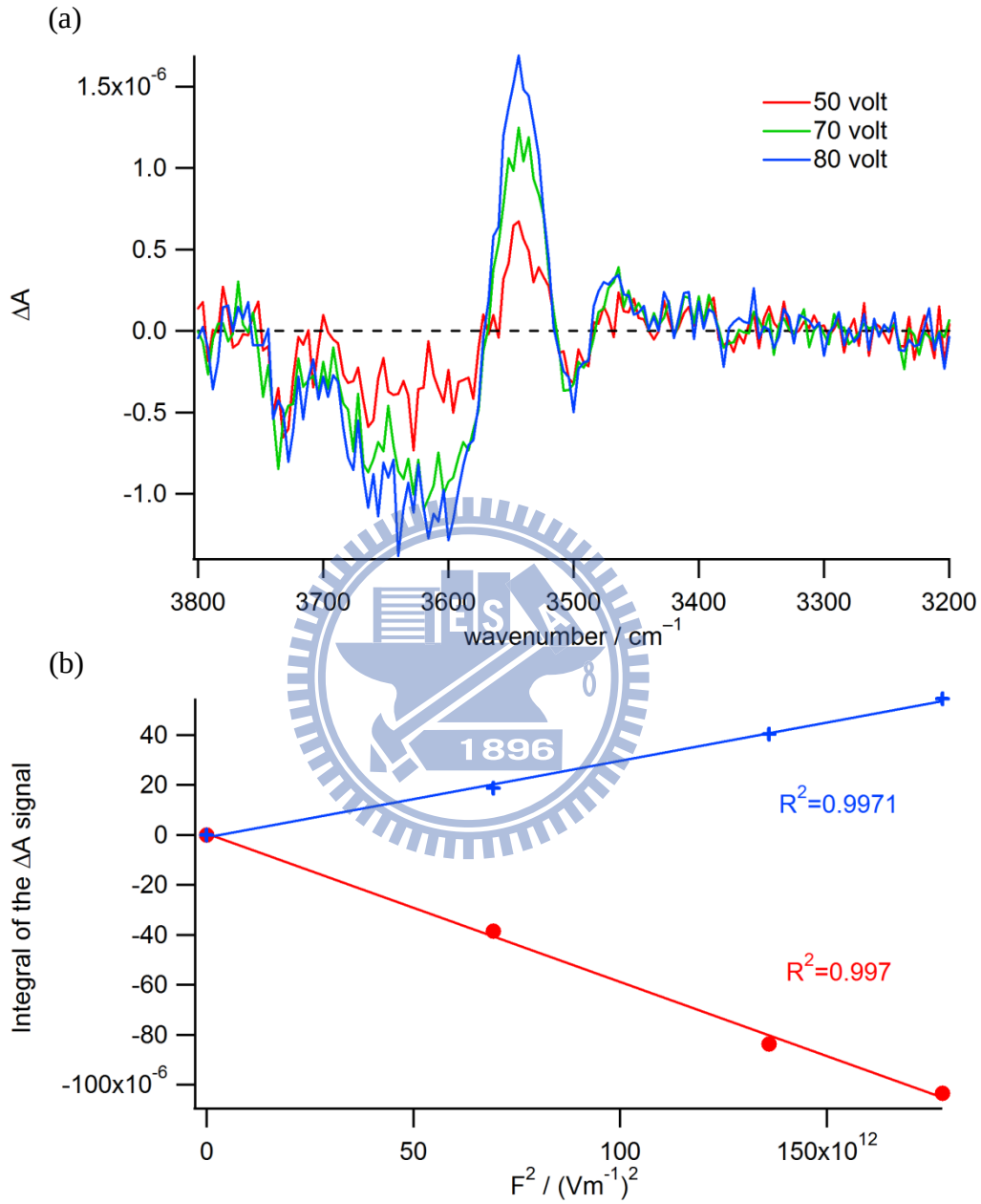

Figure IV-9. (a) The Δ*A* spectra of water in 1,4-dioxane (1.0 M) measured with 50, 70, and 80 V. (b) Plot of the integrated Δ*A* signals for the 3516–3572 (+) and 3580–3684 cm^{-1} (●) region as a function of the square of external electric field, F^2. Solid lines are a fit to a linear function having a zero intercept.

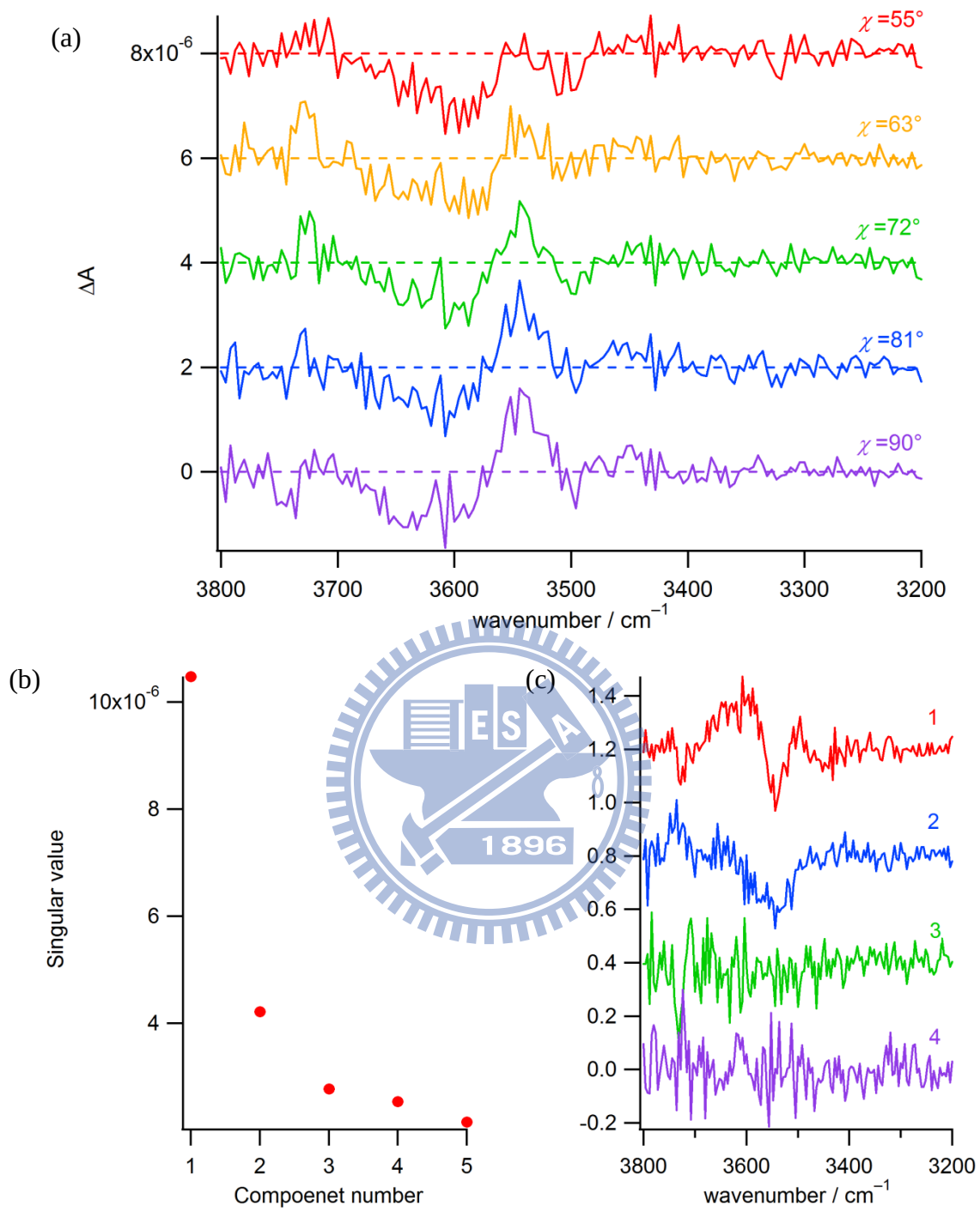

Figure IV-10. (a) IR electroabsorption spectra of water in 1,4-dioxane (1.0 M) measured at χ = 55, 63, 72, 81 and 90°. Each ΔA spectrum is offset by 2×10^{-6} for clarity of display. (b) Plot of singular values obtained from the SVD of the χ-dependence of the ΔA spectrum. (c) The spectral components corresponding to the largest four singular values.

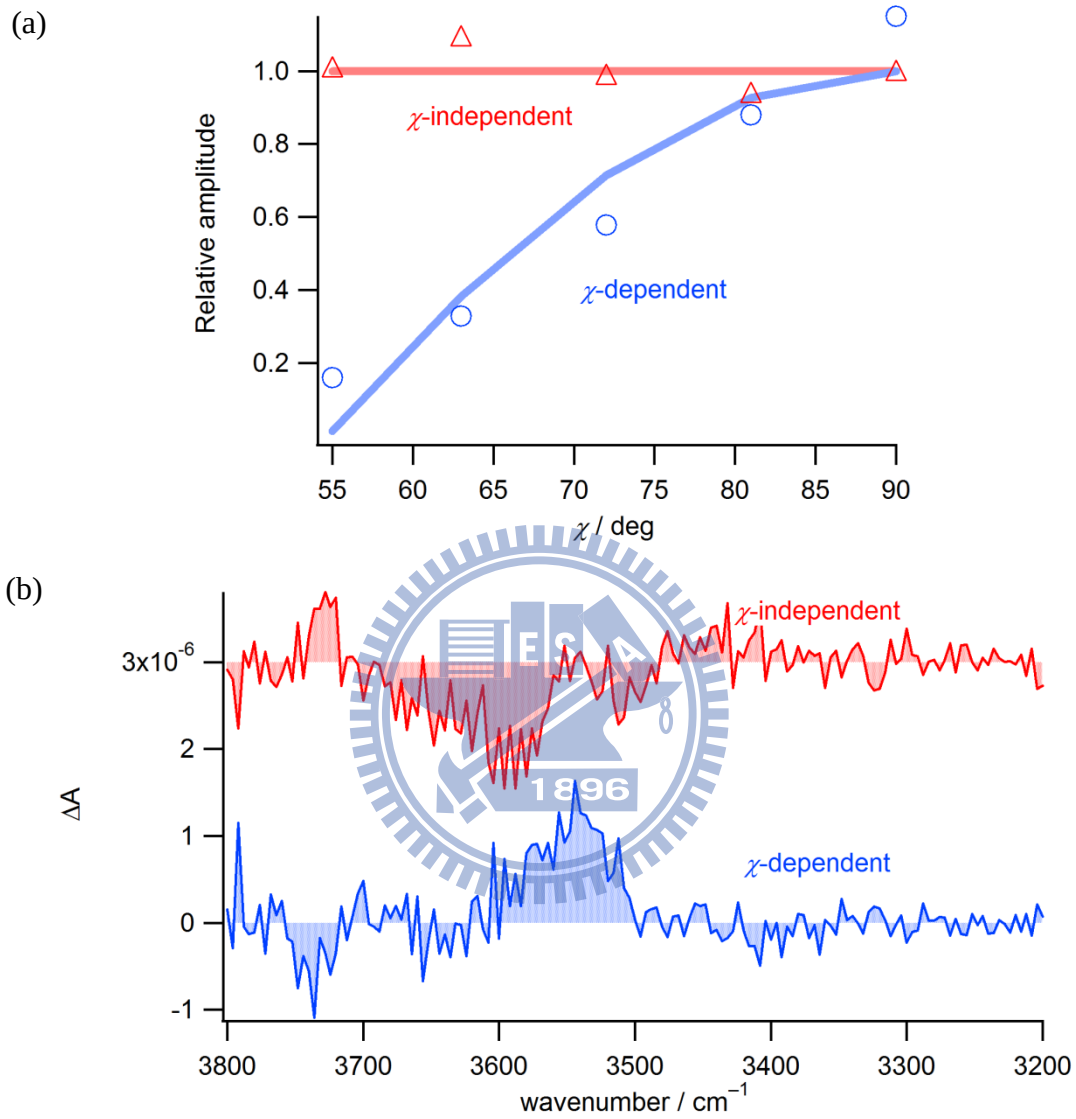

Figure IV-11. (a) Model functions (thick solid line) and reconstructed χ dependences (open triangle and circle). (b) χ-independent (red) and χ-dependent (blue) spectral components.

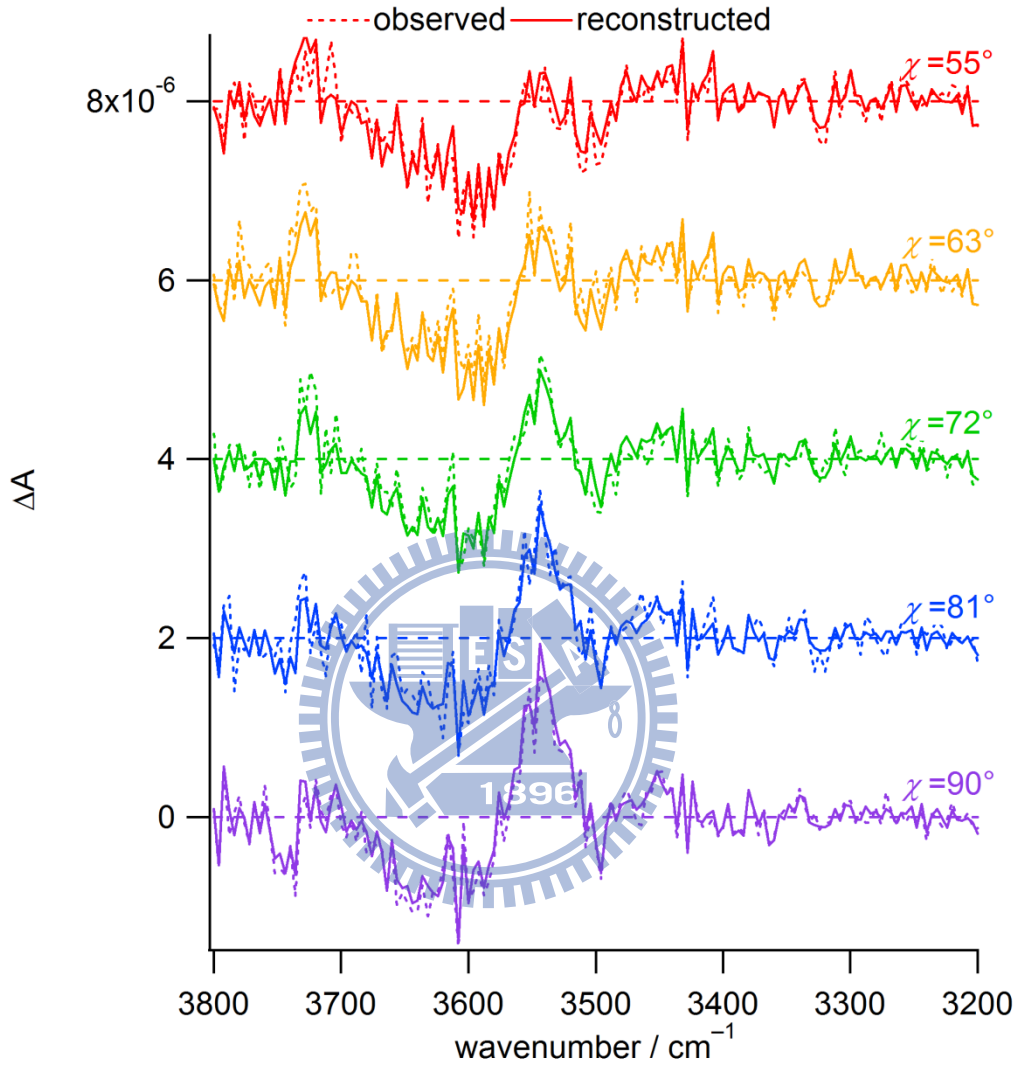

Figure IV-12. Observed (dotted line) and reconstructed (solid line) Δ*A* spectra of water in 1,4-dioxane.

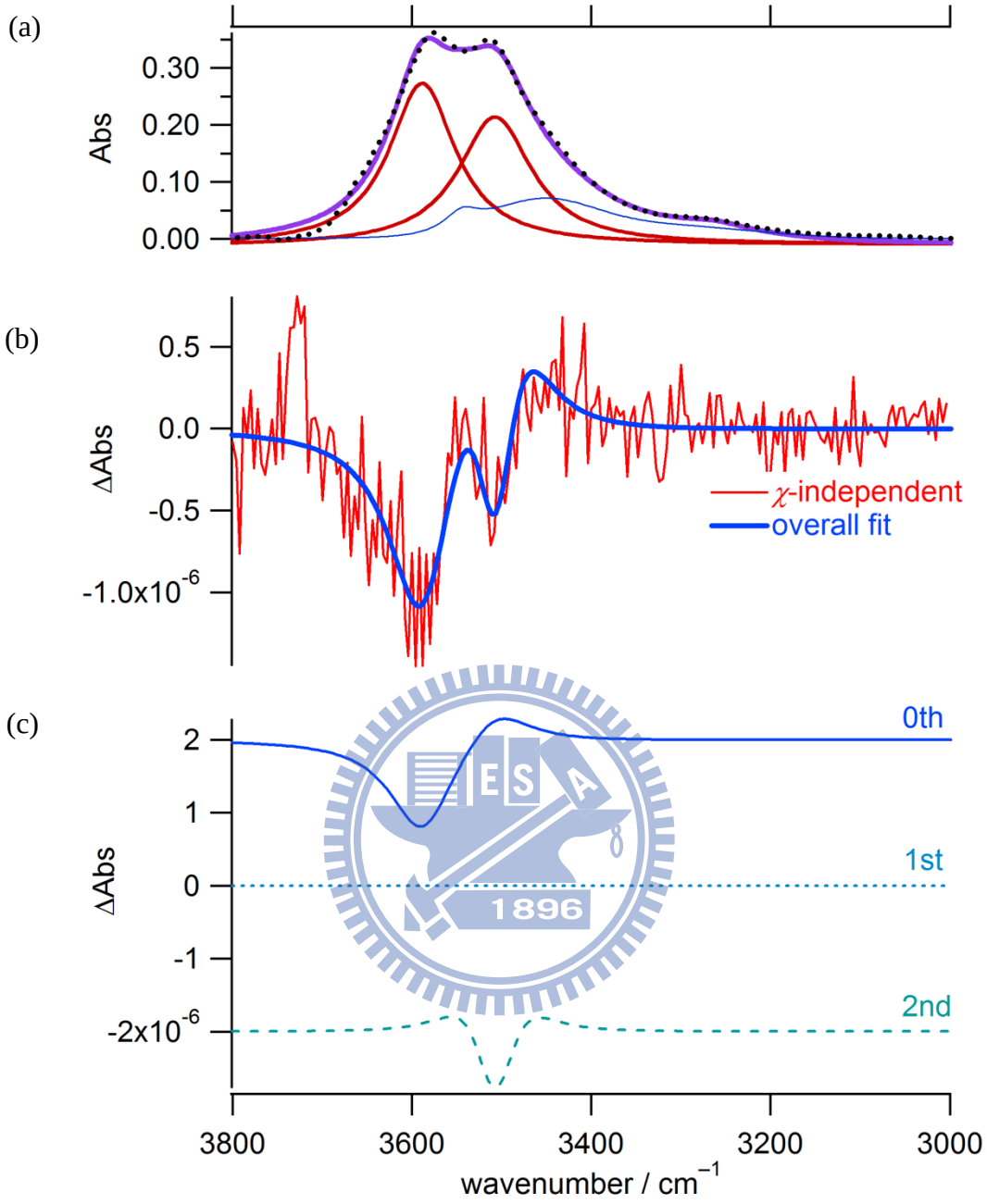

Figure IV-13. Fitted result for the χ-independent component spectrum of water in 1,4-dioxane. (a) Dotted black line, observed FT-IR spectrum; purple solid line, simulated spectrum using the results of MCR analysis (see text for details); red thick solid line, two Lorentzian bands, ν_{as}(OH) and ν_s(OH), consisting of the $\mathbf{w}_1$ spectrum; blue thin solid line, the $\mathbf{w}_2$ spectrum, which is neglected in the fit below. (b) Red line, χ-independent ΔA spectrum obtained with SVD; thick blue line, the best fit to Eq. II-24. (c) Decomposition of the overall fit into the zeroth (solid line), first (dotted line), and second (dashed line) derivative shapes.

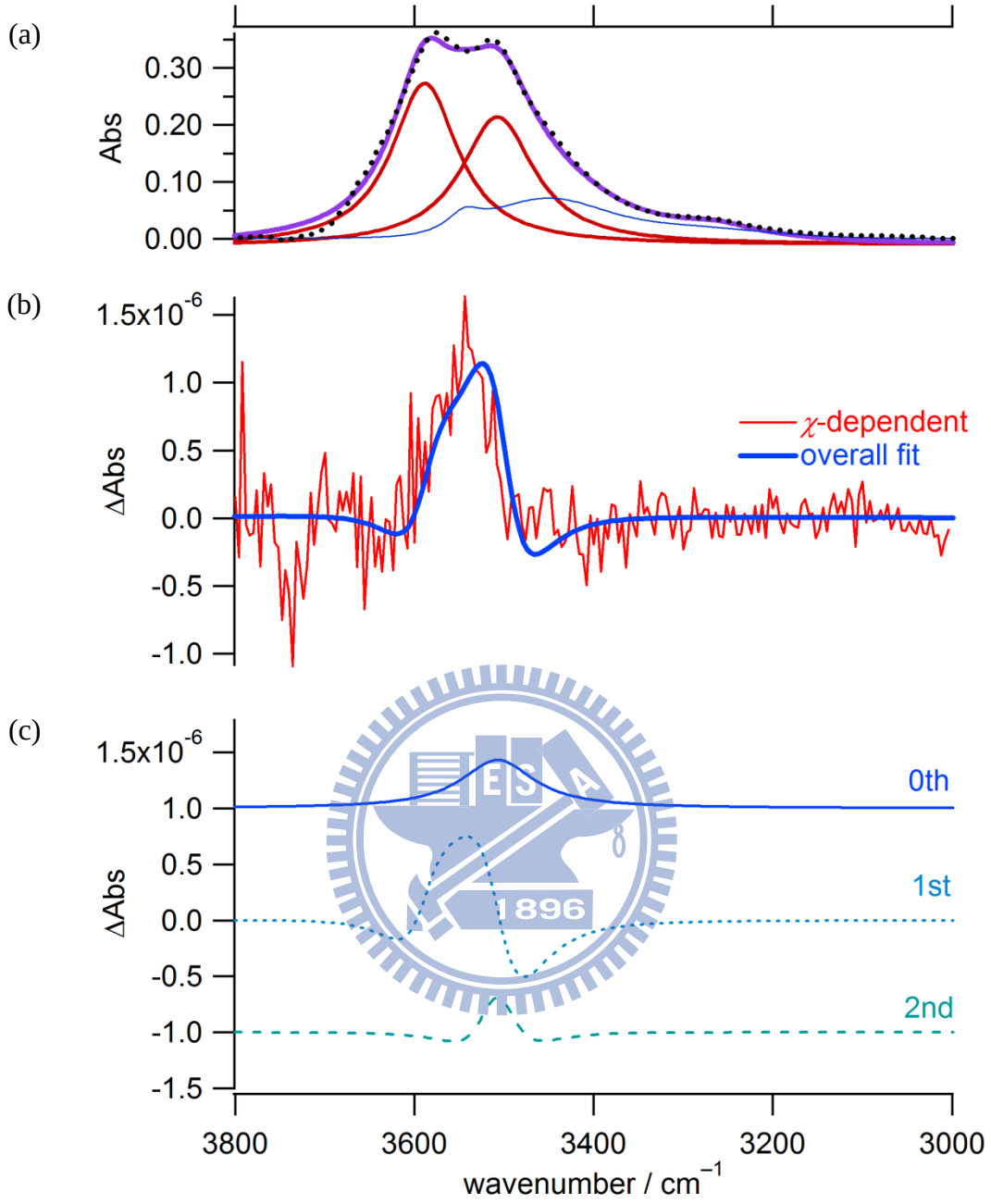

Figure IV-14. Fitted result for the χ-dependent component spectrum of water in 1,4-dioxane. (a) Dotted black line, observed FT-IR spectrum; purple solid line, simulated spectrum using the results of MCR analysis (see text for details); red thick solid line, two Lorentzian bands, ν_{as}(OH) and ν_s(OH), consisting of the $\mathbf{w}_1$ spectrum; blue thin solid line, the $\mathbf{w}_2$ spectrum, which is neglected in the fit below. (b) Red line, χ-dependent ΔA spectrum obtained with SVD; thick blue line, the best fit to Eq. II-24. (c) Decomposition of the overall fit into the zeroth (solid line), first (dotted line), and second (dashed line) derivative shapes.

Chapter V

Conclusion

In this thesis, the author presented an IR electroabsorption spectroscopic study of water dissolved in 1,4-dioxane. Water dissolved in 1,4-dioxane, although at a low concentration, is essentially different from pure water. A highly structured network of hydrogen bonding that is present in pure water is lost completely or broken to a great extent in 1,4-dioxane solution. Nevertheless, we believe that it is important as a bottom-up approach to study 1,4-dioxane solution of water, in which water may be thought of as more "free" solute molecules. Such a study can fill a huge gap lying between the gas phase and pure liquid.

First, the concentration dependence of FT-IR absorption spectra of water dissolved in 1,4-dioxane was studied in order to clarify how many water species exist in the solution. The observed concentration-dependent spectra were well-explained by assuming two water species: one is an isolated water molecule interacting solely with 1,4-dioxane, and the other is the water molecule in a small water cluster. Then, the results of IR electroabsorption measurements on the 1,4-dioxane solution of water were discussed. The dependence of the ΔA spectra on the field strength F was examined. The author performed an SVD analysis of the ΔA spectra recorded with changing the angle χ and interpreted the results in terms of the two-component model. The author found that, unlike our previous studies, the orientational polarization contribution to the ΔA spectrum of the ν(OH) band of water is not dominant; instead, ΔA signals associated with water's electronic properties such as $\Delta\boldsymbol{\mu}$, $\Delta\boldsymbol{\alpha}$, and the transition polarizability $\mathbf{A}$ play an important role in the response to an applied electric field.

References

1. Ohmine, I.; Tanaka, H. *Chem. Rev.*, **1993**, *93*, 2545.
2. Rey, R.; Moller, K. B.; Hynes, J. T. *J. Phys. Chem. A.*, **2002**, *106*, 11993.
3. Fecko, C. J.; Eaves, J. D.; Loparo, J. J.; Tokmakoff, A.; Geissler, P. L. *Science*, **2003**, *301*, 1698.
4. Bagchi, B. *Chem. Rev.*, **2005**, *105*, 3197.
5. E.T.J. Nibbering; T. Elsaesser, *Chem. Rev.*, **2004**, *104*, 1887.
6. Wang, Z.; Pang, Y. Dlott D. D. *J. Phys. Chem. A*, **2001**, *111*, 3196.
7. Stark, J. *Nature*, **1913**, *92*, 401.
8. Stark, J. *Ann. Phys.* **1914**, *43*, 965.
9. Ohta, N. *Bull. Chem. Soc. Jpn*, **2002**, ***75***, 1637.
10. Bublitz, G.U.; Boxer, S.G. *Annu. Rev. Phys. Chem*, **1997**, *48*, 213.
11. Boxer, S.G. *J. Phys. Chem. B*, **2009**, *113*, 2972.
12. Liptay, W. *Angew. Chem. Int.*, **1969**, *8*, 117.
13. Liptay, W. *In Excited States (E. C. Lim, ed.) Academic Press*, **1974**, *1*, 129.
14. Silverman, L.N. et al. *J. Phys. Chem. A*, **2008**, *112*, 10244.
15. Brewer, S.; Franzen, S. *J. Chem. Phys*. **2003**, *119* , 851
16. Yoshizawa, T. et al. *J. Phys. Chem. B*, **2004**, *108*, 19132.
17. Mehata, M.S. et al. *J. Phys. Chem. B*, **2010**, *114*, 6258.
18. Mehata, M.S. et al. *J. Photochem. Photobio. a-Chem.*, **2009**, *204*, 39.
19. Handler, P.; Aspnes, D.E. *J. Chem. Phys.*, **1967**, *47*, 473.
20. Chattopadhyay, A.; Boxer, S.G. *J. Am. Chem. Soc.*, **1995**, *117*, 1449.
21. Andrews, S.S.; Boxer, S.G. *J. Phys. Chem. A*, **2000**, *104*, 11853.
22. Park, E.S.; Boxer, S.G. *J. Phys. Chem. B*, **2002**, *106*, 8910.
23. Hiramatsu, H.; Hamaguchi, H. *Appl. Spec.*, **2004**, *58*, 355.
24. Hiramatsu, H.; Kato, C.; Hamaguchi, H. *Chem. Phys. Lett.*, **2001**, *347*, 403.

25. Hiramatsu, H.; Hamaguchi, H. *Chem. Phys. Lett.*, **2002**. *364*, 457.

26. Min, Y.K.; Hiramatsu, H.; Hamaguchi, H. *Chem. Lett.*, **2002**, *1*, 68.

27. Shigeto, S.; Hiramatsu, H.; Hamaguchi, H. *J. Phys. Chem A.*, **2006**, *110*, 3738.

28. Lee, I.C.; Hamaguchi, H.; Shigeto, S. *Chem. Phys. Lett.*, **2008**, *466*, 144.

29. Wang, W. C.; Shigeto, S. *J. Phys. Chem. A*, **2011**, *115*, 4448.

30. Jalviste, E.; Ohta, N. *J. Photochem. Photobio. C-Photochem. Rev.*, **2007**, *8*, 30.

31. Poner, M.; Mathles, R. *J. Phys. Chem.*, **1983**, *87*, 5090.

32. Sarah, A. Locknar; Linda, A. Peteanu *J. Phys. Chem. B*, **1998**, *102*, 4240.

33. Å kerlöf, Gösta; Short, Oliver A. *J. Am. Chem. Soc.*, **1936**, *58*, 1241.

34. Middendorf, T.R.; et al. *Biochimica Et Biophysica Acta*, **1993**, *1143*, 223.

35. Premvardhan, L.L.; Peteanu,L.A. *J. Phys. Chem. A*, **1999**, *103*, 7506.

36. McClellan, A. L. *Table of Experimental Dipole Moments*; Freeman, W. H.; San Francisco and London, **1963**

37. M. L. Cowan; B. D. Bruner, N. Huse; J. R. Dwyer; B. Chugh; E. T. J. Nibbering; T. Elsaesser; R. J. D. Miller. *Nature*, **2005**, *434*, 199.

38. Stratt, R.M.; Maroncelli, M. *J. Phys. Chem.*, **1996**. *100*, 12981.

39. Berberian, J.G. *J. Molecular Liquids*, **1993**, *56*, 1.